Stem Cell Research & Therapy

RESEARCH Open Access

Single-cell transcriptomics reveals notch regulation in quiescent LEPR⁺ endometrial mesenchymal stem cells

Yuan Fang[1,2†], Dandan Cao[2†], Cheuk-Lun Lee[1,3], Philip C. N. Chiu[1,2], Ernest H. Y. Ng[1,2], William S. B. Yeung[1,2*] and Rachel W. S. Chan[1,2*]

Abstract

Background The human endometrium is a regenerative tissue relying on stem/progenitor cells. Endometrial mesenchymal stem cells (eMSCs) are typically enriched using perivascular markers like CD140b and CD146. However, the identity of more primitive and quiescent eMSC subpopulations remains unclear.

Methods We performed single-cell RNA sequencing (scRNA-seq) on cultured CD140b⁺CD146⁺ eMSCs and integrated this with published scRNA-seq data of primary human endometrial cells. We identified a LEPR⁺ subpopulation and analyzed its characteristics through in vitro assays, flow cytometry, immunostaining, and bioinformatic tools including cell–cell interaction analysis and pseudotime trajectory inference.

Results A LEPR⁺ eMSC subpopulation was found to reside at the root of the differentiation trajectory and showed high expression of Notch receptors. These cells exhibited quiescent features, resided predominantly in the G0 phase, and demonstrated superior clonogenic and self-renewal capacity compared to LEPR⁻ eMSCs and bulk eMSCs. Notch signaling, particularly via JAG1 and DLL1, was implicated in maintaining the LEPR⁺ phenotype and quiescence.

Conclusions LEPR⁺ eMSCs represent a primitive, quiescent subset of human endometrial stem cells. Notch signaling maintains their stemness and quiescence, suggesting therapeutic relevance for endometrial regeneration.

Keywords Endometrial stem cells, Leptin receptor, Single-cell RNA sequencing, Stem cell quiescence, Clonogenic, Notch signaling, Endometrial regeneration, Mesenchymal stem cells, Human endometrium, Quiescent, Clonogenic

Introduction

Adult stem cells (ASCs) are a population of cells essential for tissue homeostasis, with abilities to self-renew and differentiate into tissue-specific cells [1, 2]. In various tissues, the stem cell population is heterogeneous, comprising a mixture of stem cells and progenitor cells [3]. Dynamic heterogeneity is considered as a strategy contributing to the self-renewal of adult stem cells [4].

The cyclical shedding, proliferation, and differentiation of the human endometrium leads to the hypothesis that stem/progenitor cells are responsible for this remarkable regeneration. In the past two decades, the existence

†Yuan Fang and Dandan Cao contributed equally to this manuscript

*Correspondence:
William S. B. Yeung
wsbyeung@hku.hk
Rachel W. S. Chan
rwschan@hku.hk
[1]Department of Obstetrics and Gynaecology, School of Clinical Medicine, Li Ka Shing Faculty of Medicine, LKS Faculty of Medicine, The University of Hong Kong, Hong Kong SAR 999077, China
[2]Shenzhen Key Laboratory of Fertility Regulation, The University of Hong Kong Shenzhen Hospital, Shenzhen 518000, China
[3]Department of Health Technology and Informatics, The Hong Kong Polytechnic University, Hong Kong SAR 999077, China

of endometrial stem/progenitor cells have been proven [5–7]. Schwab and Gargett demonstrated that the combination of two perivascular markers CD140b (PDGFRβ) and CD146 (MCAM) could be used to enrich human endometrial mesenchymal stem cells (eMSCs) [8]. The $CD140b^+CD146^+$ eMSC population exhibits properties similar to those of mesenchymal stem cells (MSCs) in multiple organs, including colony-forming ability, fibroblast-like morphology, multipotency, as well as their perivascular location [8, 9].

Using high-throughput transcriptomics technology, we and others have mapped human endometrial cells from multiple dimensions and perspectives at single-cell resolution [10–12]. Single-cell RNA sequencing (scRNA-seq) measures the transcriptome of each cell in a sample and unbiasedly classifies the cells into different subtypes, which reflect cellular heterogeneity within the sample [13, 14]. The technology enables identification of new stem cell types and their interactions with other cells in the population [15, 16].

ASC quiescence is regulated by distinct molecular mechanisms involving intrinsic factors within the cells and extrinsic cues from their microenvironment [17]. Extrinsic factors, such as Notch signaling, can play a vital role in maintaining ASC quiescence [18, 19]. Notch signaling significantly directs cell fate decisions and maintains stem cell homeostasis [20]. Additionally, it inhibits differentiation and fosters the preservation of a self-renewing state across various cell types [21]. Bjornson et al. revealed quiescent muscle stem cells (MuSCs) exhibit activation of Notch signaling. Selective removal of the recombining binding protein-Jκ (RBP-Jκ), a nuclear factor essential for Notch signaling, resulting in depletion of the MuSC pool [22]. Our research group demonstrated activation of Notch signaling more effectively maintained quiescence in eMSCs. Yet, these quiescent eMSCs could resume the cell cycle based on the Notch and Wnt signaling cues in the microenvironment [23].

In this study, we performed scRNA-seq to systematically analyze $CD140b^+CD146^+$ eMSCs and identified a primitive subpopulation that highly expresses the leptin receptor (LEPR). The $LEPR^+$ eMSCs marked the initiation of the differentiation trajectory of eMSCs. Functionally, $LEPR^+$ eMSCs exhibited superior stem cell properties compared to $LEPR^-$ eMSCs and bulk eMSCs. Bioinformatics analysis of a primary human endometrial single-cell dataset revealed that $LEPR^+$ eMSCs were the most communicative subpopulation among endometrial cells. Notably, $LEPR^+$ eMSCs from fresh endometrial tissue were predominantly in the G0 phase of the cell cycle, representing the first identification of quiescent stem cells with known surface markers in human endometrial tissue. Moreover, these quiescent $LEPR^+$ eMSCs exhibited high expression of Notch receptors, and further investigations revealed their co-localization with Notch ligands JAG1 and DLL1, suggesting that Notch signaling plays a crucial role in maintaining the quiescent state of these cells.

Materials and methods

Human endometrial tissues

Endometrial tissues (n = 35) were collected from women who were aged 32–52 years with regular menstrual cycles and had not taken exogenous hormones 3 months before undergoing hysterectomy for fibroids or adenomyosis in Queen Mary Hospital, Hong Kong and the University of Hong Kong-Shenzhen Hospital, Shenzhen (Supplementary Table S1). Ethics approval of the study was granted from the Institutional Review Board of The University of Hong Kong/Hospital Authority Hong Kong West Cluster (UW20-465) and The Institutional Review Board of the University of Hong Kong-Shenzhen Hospital ([2018]94). Informed written consent was obtained from each woman prior to the study procedure.

Isolation of eMSC from human endometrium

Human endometrial tissue was minced and dispersed into single cell suspensions with phosphate-buffered saline (PBS) containing collagenase type III (0.3 mg/ml, Worthington Biochemical Corporation, USA, #LS004182) and deoxyribonuclease type I (40 μg/ml, Worthington Biochemical Corporation, #LS002139) in a shaking water bath for 1 h at 37 °C as described [23]. After two rounds of enzymatic digestion, the dispersed cells were filtered through 40 μm sieves (BD Bioscience, USA). Ficoll-Paque (Cytiva, Sweden) density-gradient centrifugation and anti-CD45-antibody-coated Dynabeads (Invitrogen, USA, #11153D) were used to remove the red blood cells and leukocytes, respectively from the dispersed cell suspension. Stromal cells were separated from the epithelial cells by negative selection using microbeads coated with anti-CD326 antibody (epithelial cell marker) (Miltenyi Biotech, Germany, #130–061-101). The purified stromal cells were seeded onto 100 mm dishes coated with fibronectin (1 mg/ml, Invitrogen, USA, #33,016–015) and cultured in growth medium (GM) containing 10% FBS, 1% antibiotic- antimycotic solution, and 1% L-glutamine in DMEM/F12. Freshly isolated and cultured endometrial stromal cells (Passage 1—3) were used in this study. Isolation of $CD140b^+CD146^+$ eMSCs was conducted as described [9]. After reaching 80% confluence in culture, endometrial stromal cells were incubated with Phycoerythrin (PE)-conjugated anti-CD140b antibody (R&D Systems, USA, #FAB1263P) at 4 °C for 45 min, and then with anti-mouse IgG1 magnetic microbeads (Miltenyi Biotech, #130–047-102) at 4 °C for 15 min. The $CD140b^+$ cells were retained in the MS columns (Miltenyi Biotech) with a magnetic

field and were collected for culture. After expansion in culture for 7–10 days in GM to allow degradation of the microbeads, the CD140b$^+$ cells were incubated with anti-CD146 microbeads (Miltenyi Biotech, #130–093-596) at 4 °C for 15 min to obtain the CD140b$^+$CD146$^+$ eMSCs.

Single-cell RNA-seq of eMSCs

Single cells were encapsulated in emulsion droplets, and scRNA-seq libraries were generated using the Chromium™ Single Cell 3' Reagent Kits v2/v3 and the Chromium™ Single Cell A/B Chip Kit according to the manufacturer's protocol. The libraries were sequenced on an Illumina NovaSeq 6000 sequencer at the Genomics Core, Centre for PanorOmic Sciences (CPOS), The University of Hong Kong [12].

Single-cell RNA-seq data analysis on eMSCs

Analysis of the scRNA-seq data was performed as described [12]. The sequencing data (FASTQ files) was processed using the 10 × Genomics cellranger pipeline (v3.0.2). High quality sample-specific FASTQ files were aligned to the human reference genome and transcriptome (GRCh38-3.0.0) using the STAR aligner (cellranger count). Aligned reads were filtered for valid cell barcodes and unique molecular identifiers (UMIs). The generated files for each sample from the cellranger v3 pipeline were loaded into the R package Seurat (version 3.2.3). Quality control and filtering steps were performed to remove outlier cells and genes. Specifically, cells were excluded if the library size, number of expressed genes or mitochondrial reads > 3 MAD (median absolute deviation). Genes were excluded if they were expressed in less than 3 cells. Additionally, ribosomal and mitochondrial genes were excluded from the analysis. Expression levels for each transcript were determined using the number of unique molecular identifiers (UMI) assigned to the transcript. Filtered cells from all the samples were merged for downstream analysis. The logNormalize method was used to normalize cell–cell expression variation. Principal component analysis was performed on the filtered and normalized gene expression matrix, and the first 50 principal components that explained the majority of variance in the data were retained. Batch effect was removed using fastMNN incorporated in the Seurat package. The K-nearest neighbor (KNN) modularity optimization-based clustering of individual cells was applied in the Seurat package. To visualize cell distribution and gene expression pattern in each cell in a low dimensional space, the Uniform Manifold Approximation and Projection (UMAP) were generated using the reduced dimensional data after batch correction. Differential expression analysis was performed using the Wilcoxon rank-sum test between each cluster and the remaining clusters. Cell cycle phase classification of each cell was performed using the CellCycleScoring function implemented in the Seurat package. Monocle2 was used to order cells in pseudotime based on the highly variable genes which were used in the Seurat package for clustering across the cells comprising SP 1–5.

Single-cell RNA-seq data analysis on human endometrium

The raw data of a published 10X single-cell RNA-seq data of human endometria from 10 healthy donors without uterine pathology were downloaded from NCBI's Gene Expression Omnibus (GSE111976) and Sequence Read Archive (SRP135922) [10]. The R package Seurat (version 4.0) was used for data scaling, transformation, clustering, dimensionality reduction, differential expression analysis and visualization [24]. The quality of cells was assessed based on three metrics: [1] number of detected genes per cell; (2) number of detected UMI per cell; (3) proportion of mitochondrial gene counts. Low-quality cells were filtered with the following criteria: gene number < 200 or > 10,000, UMI > 1000, mitochondrial gene proportion > 0.3. All samples were merged and batch-effect was removed with the use of harmony (v.0.1.1) [25]. The filtered gene-cell matrix was first normalized using the 'LogNormalize' method in package Seurat (version 4.0) with default parameters. The top 2,000 variable genes were identified using the 'vst' method of Seurat FindVariableFeatures function. PCA was performed using the top 2,000 variable genes. UMAP was performed on the top 30 principal components for visualizing the cells. Graph-based clustering was performed on the PCA-reduced data for clustering analysis with the package Seurat (version 4.0). The resolution was set to 0.6 to obtain a finer result. Briefly, the first 30 principal components of the integrated gene-cell matrix were used to construct a shared nearest-neighbor graph (SNN; FindNeighbors() in Seurat), which was used to cluster the dataset (FindClusters()) using a graph-based modularity-optimization algorithm of the 'Louvain' method for community detection. Wilcoxon rank sum test in FindMarkers() of Seurat was used to perform differential gene expression analysis. GO and Pathway analysis were performed with the R package clusterProfiler3 [26], which supports statistical analysis and visualization of functional profiles for genes and gene clusters. CellPhoneDB was used to infer cell–cell communication network by expression of ligand-receptor [27].

Single-cell datasets integration and analysis

Two preprocessed single-cell RNA-seq datasets, consisting of our cultured eMSC dataset and a primary human endometrial dataset, were integrated to enable a comprehensive analysis of cellular populations. To address batch effects between the datasets, the Harmony algorithm [25] was applied. Dimensionality reduction was performed

using PCA on the integrated gene-cell matrix to capture the major sources of variation. For clustering analysis, the first 30 principal components were utilized to construct a shared nearest-neighbor graph (SNN; FindNeighbors() in Seurat), followed by clustering with the Louvain algorithm via FindClusters() to refine cellular groupings and identify subpopulations.

Cells were annotated based on pre-defined cell clusters from the original preprocessing steps of each dataset. These pre-existing annotations were retained to ensure consistency with prior analyses. For pseudotime trajectory analysis, Monocle 3 [28] was used to infer dynamic cellular processes and lineage differentiation.

Cell sorting and flow cytometry

FACS using CD146, PDGFRβ and LEPR on freshly isolated human endometrial cells

Sorting of fresh endometrial cells was performed on the day of tissue isolation. After dissociation of the endometrial tissues with collagenase, the dispersed cells were passed through a 40 μm sieve, and red blood cells were removed by gradient centrifugation using Ficoll Paque. The single cell suspensions were successively incubated with Zombie Aqua™ (Biolegend, USA, #423,101) in PBS for 10 min on ice in the dark, with APC-conjugated anti-PDGFRβ antibody, PerCP/Cyanine5-conjugated anti-CD146 antibody, PE-conjugated anti-LEPR antibody, Alexa Fluor 700-conjugated anti-CD45 antibody and PE/Cyanine7-conjugated anti-CD326 antibody in 0.5% BSA/PBS for 45 min at 4 °C in the dark (Supplementary Table S2). Cell sorting was performed on a FACSAria™ III Cell Sorter (BD Biosciences) at the core laboratory of The University of Hong Kong-Shenzhen Hospital. Fluorescence Minus One (FMO) controls were included with the anti-LEPR, anti-CD146 and anti-PDGFRβ antibodies. Data were analyzed by the FlowJo Software (Tree Star Inc). The gating strategies for different stromal subsets are shown in Supplementary Figure S8.

Cell cycle analysis on freshly isolated endometrial cells

Single cell suspensions of freshly isolated endometrial cells were incubated with the respective antibodies described above. The stained cells were resuspended in the Fixation/Permeabilization solution (BD Bioscience, #554,714) for 20 min on ice. After permeabilization, the cells were incubated with PerCP/Cyanine5 conjugated anti-Ki67 antibody (Supplementary Table S2) in 1X Perm/Wash™ buffer (BD Bioscience) for 1 h at room temperature and then with Hoechst 33,342 (ThermoFisher Scientific, #3,143,066) for 10 min on ice. FMO controls were included for each antibody and dye, and compensation was performed using single-stained compensation beads (Invitrogen). Cells were analyzed by a CytoFLEX flow cytometer (Beckman Coulter Inc.) using the FlowJo software (Tree Star).

Detection of HES-1 on freshly isolated endometrial cells

Freshly isolated endometrial cells were incubated with Zombie Aqua™ in PBS for 10 min on ice in the dark. Subsequently, they were incubated with six surface marker antibodies (Supplementary Table S2), along with the BV510-conjugated anti-CD326 antibody and BV510-conjugated anti-CD45 antibody in 0.5% BSA/PBS for 45 min at 4 °C in the dark. The cells were then resuspended in 1 ml of True-Nuclear™ 1X Fix Concentrate (Biolegend, #424,401) and incubated for 1 h at room temperature. After fixation, cells were mixed with 2 ml of True-Nuclear™ 1X Perm Buffer (Biolegend, #424,401) and resuspended in 1X Perm Buffer. Following permeabilization, the cells were incubated with the anti-HES-1 antibody (Supplementary Table S2) for 1 h at room temperature. Compensation for fluorescence spillover was performed using single-stained compensation beads (Invitrogen). Finally, the cells were analyzed by a CytoFLEX flow cytometer (Beckman Coulter Inc.) and the FlowJo software (Tree Star).

FACs using CD146, PDGFRβ and LEPR on cultured human endometrial stromal cells

Cultured endometrial stromal cells (P1-3) were incubated with APC-conjugated anti-PDGFRβ, FITC-conjugated anti-CD146, and PE-conjugated anti-LEPR antibodies (Supplementary Table S2) in 0.5% BSA/PBS for 45 min at 4 °C in the dark. Cell sorting was performed using the FACSMelody Cell Sorter (BD Biosciences) at the Imaging and Flow Cytometry Core, CPOS, The University of Hong Kong using the BD diva software (BD Biosciences) or FACSAria™ III Cell Sorter (BD Biosciences) at the Core laboratory, The University of Hong Kong-Shenzhen Hospital. For analyzing cell properties, flow cytometry was performed on a CytoFLEX flow cytometer (Beckman Coulter Inc.). FMO controls were included for each antibody. Data were analyzed using the FlowJo software (Tree Star). The gating strategies to identify different stromal subsets are shown in Supplementary Fig S7.

Immunohistochemistry

Paraffin sections (5 μm) from human endometrial tissues were dewaxed with xylene, rehydrated in descending alcohol series and water before antigen retrieval using the antigen retrieval buffer (Dako, USA, #S169984) in a microwave oven. The sections were then incubated with 0.3% hydrogen peroxide for 10 min, blocked with 5% BSA/PBS for 30 min, and further incubated with the anti-LEPR antibody (Supplementary Table S3) or isotype-matched control antibody diluted in 0.1% BSA/PBS overnight at 4 °C. The sections were then successively

incubated with the biotinylated secondary antibody (Supplementary Table S3) for 1 h and with Vectastain ABC reagent (Vector Laboratories, USA, #PK-6100) for 30 min before examination under a Zeiss Axioskop II microscope (Carl Zeiss) for colour development with 3,3'-daminobenzidine (Dako, K3467). Nuclei were counterstained with hematoxylin for 30 s and washed with distilled water. The slides were mounted with an aqueous mounting medium (Dako, S3025), and images were captured using a Photometrics CoolSNAP digital camera (Roper Scientific).

Triple immunofluorescence staining

After dewaxing and antigen retrieval as described above, tissue sections were incubated with 3% hydrogen peroxide for 10 min before permeabilization by 0.1% Triton X-100 for 10 min and blocking of non-specific binding with 5% BSA/PBS for 1 h. The sections were incubated with primary antibodies (Supplementary Table S3) at 4 °C overnight, followed by incubation with secondary antibodies (Supplementary Table S3) for 1 h. The sections were then washed, counterstained with DAPI, mounted using an anti-fade fluorescence mounting medium (Dako, #S3023) and were washed with PBST. All the above steps were conducted at room temperature. Multi-spectrum fluorescence images were acquired by the Zeiss confocal microscope (Carl Zeiss LSM 880), using the LSM ZEN (Zen 3.2, blue edition) software (Carl Zeiss, Germany) at the Imaging and Flow Cytometry Core, CPOS, The University of Hong Kong. For quantification analysis, at least 500 cells from each sample were counted.

Multiplexed immunohistochemistry

Multiplexed immunohistochemistry (mIHC) was performed on 4-μm-thick formalin-fixed, paraffin-embedded whole tissue sections using sequential staining with standard primary antibodies, in combination with a TSA 7-color kit (Absinbio, China, #abs50015-100 T). DAPI staining was subsequently applied. After deparaffinization, the slides were incubated overnight at 4 °C with primary antibodies listed in Supplementary Table S3, followed by 10 min incubation with horseradish peroxidase (HRP)-conjugated secondary antibodies (anti-rabbit/mouse HRP, Absinbio, #abs50015-02, or anti-goat HRP, Supplementary Table S3). Fluorescent labeling was developed for 10 min according to the manufacturer's instructions for each TSA reagent, then transferred to preheated citrate solution (90 °C) and subjected to heat treatment in a microwave at 20% maximum power for 15 min. The slides were cooled to room temperature in the same solution. Slides were washed with Tris buffer between all steps. This process was repeated for the following antibodies and corresponding fluorescent dyes: anti-PDGFRβ/TSA 570, anti-DLL1/TSA 690, anti-CD146/TSA 520, anti-JAG1/TSA 480, and anti-LEPR/TSA 620. Finally, DAPI (Absinbio, #abs47047616) was applied (2 drops per slide), followed by washing in distilled water and coverslip. After air drying, the slides were imaged using the Pannoramic MIDI II system (3DHISTECH), and the images were analyzed with Indica Halo software.

In vitro colony-forming assay

Cell sorted populations of endometrial stromal cells were seeded in triplicates at clonal density (300 cells per well) onto fibronectin-coated plates and cultured in GM for 15 days in a humidified incubator at 37℃. Medium was changed every 7 days, and the colonies were monitored regularly to ensure that they were derived from single cells. The number of colonies formed was evaluated on day-15 by toluidine blue (1 mg/ml, Sigma-Aldrich) staining. Clones ≥ 50 cells were counted. Cloning efficiency was determined by the number of colonies divided by the number of seeded cells multiply by 100.

In vitro serial cloning assay

Large colonies (> 4000 cells) derived from the sorted populations of stromal cells were trypsinized using cloning rings (Sigma-Aldrich). The cell number of each clone was determined and the cells were reseeded at a density of 300 cells per well in 6-well plates [9].

Mesenchymal lineages differentiation assay

In vitro differentiation

In vitro differentiation was performed to compare multipotency of the sorted stromal subsets (eMSC, $LEPR^-$ eMSC, and $LEPR^+$ eMSC) as described [29]. The clonally derived cells from each stromal subset of different patients were pooled and expanded. For adipogenic and osteogenic lineages, the cells were re-seeded into 6-well plates and cultured in the respective differentiation induction medium. For chondrogenic lineage differentiation, 5×10^5 cells were prepared into cell pellets and cultured in chondrogenic induction medium in 15 ml Falcon tubes. The adipogenic induction medium was changed every 3 days, and the cells were cultured for 18 days. The osteogenic induction medium and chondrogenic medium were changed weekly and cultured for 4 weeks. Stromal cells cultured in GM only from each subset were used as the negative control. To assess the differentiation, cells were histochemically stained with oil red O and immunocytochemistry using antibodies against PTHR1 and collagen X (Supplementary Table S4) for adipogenic, osteogenic and chondrogenic differentiation, respectively.

Real-time RT-PCR

Expression of lineage marker genes was detected using quantitative real-time polymerase chain reaction (qPCR)

with Taqman probes (Supplementary Table S4). Total RNA was extracted from induced differentiated cells and control cells using the Absolutely RNA microprep kit (Stratagene, USA, #400,805), and RNA was reverse transcribed to cDNA using the High Capacity cDNA Reverse Transcription Kit (Applied Biosystem, USA, #4,374,966). Results were calculated based on the comparative $2^{-\Delta\Delta ct}$ method. The induced cells of each subset were compared to their control group separately, and the fold changes were normalized to the eMSC group.

Western blot

Proteins were extracted from samples with cell lysis buffer (Ambion, USA). The protein samples were mixed with 5X sodium dodecyl sulfate loading buffer, denatured at 95 °C for 10 min and loaded in amount according to their concentration in the samples. The samples were subjected to sodium dodecyl sulfate–polyacrylamide gel electrophoresis, and the resolved proteins were transferred to polyvinylidene fluoride (PVDF) membranes. The membranes were blocked with 5% nonfat milk (Nestle, Switzerland) in PBS containing 0.1% Tween-20 (PBST) for 30 min before incubation with the respective primary antibodies overnight at 4 °C (Supplementary Table S5) followed by incubation with horseradish peroxidase-conjugated secondary antibody (Supplementary Table S5) for 1 h at room temperature. Protein bands were visualized by enhanced cavity-based chemiluminescence (Westsave UP™; AbFrontier, Korea, #LF-QC0101). The expression of target proteins was calculated relative to the housekeeping protein β-actin. The fold change was determined after normalization to the eMSC group.

Real-time RT-PCR for quiescent markers

Cellular quiescence was assessed by the expression of quiescence genes (Supplementary Table S6) using qPCR, glyceraldehyde 3-phasephate dehydrogenase (GAPDH) as an internal reference. Total RNA was extracted from cell-sorted endometrial stromal subsets using the RNeasy micro kit (Qiagen, USA, #74,104). The extracted RNA was then reverse transcribed into cDNA with the aid of the HiScript III All-in-one RT SuperMix Perfect for the qPCR Reverse Kit (Vazyme, China, #R333-01). Real-time PCR was carried using an ABI 7500 Real-Time PCR system (Life Tech, USA) using SYBR Green Reagents (TaKaRa, Japan). The results were calculated using the comparative $2^{-\Delta\Delta ct}$ method and normalized to the eMSC group.

Statistical analysis

All statistical analyses were performed using the GraphPad PRISM software (version 8.2.0; GraphPad Software Inc., USA) and tested for normal distribution using the Shapiro–Wilk test. Mann–Whitney test was performed to determine the statistical significance between the two groups. Kruskal–Wallis test followed by Dunn's post hoc test was used for multiple group comparisons. Data are presented as mean ± SD. Results were considered statistically significant when $P < 0.05$.

Results

Expression of LEPR in subpopulation-3 from single-cell sequencing dataset of cultured eMSCs

$CD140b^+CD146^+$ eMSCs were collected from a full-thickness endometrial sample at secretory phase of menstrual cycle after enzymatic dispersion (Fig. 1A) and serial magnetic microbeading [9]. A portion of the $CD140b^+CD146^+$ cells (S3) were used for scRNA-seq. Another portion of the cells were cultured at low seeding density, and the clones formed after 15 days were harvested as differentiated eMSCs (S3C) and processed for scRNA-seq. In total, two single-cell libraries were subjected to scRNA-seq on a 10X genomics platform. After quality control of the raw sequencing tags, around 5×10^8 sequence reads from each sample were obtained. 73% of the data confidently and 76% of the data uniquely mapped to the human reference transcriptome GRCh38 (NCBI). Finally, we obtained 1,101 and 2,499 high-quality cells from S3 and S3C, respectively in the final dataset.

The Seurat analysis pipeline was applied to the dataset. After batch correction, clustering analysis of the scRNA-seq data revealed 5 subpopulations (SP0-4) containing 1013 SP0 (28.1%), 896 SP1 (24.9%), 670 SP2 (18.6%), 658 SP3 (18.3%) and 363 SP4 (10.1%) cells (Fig. 1B). Pearson correlation analysis on the 5 SPs based on average gene expression analysis revealed that SP4, SP0 and SP2 had closer mutual expression distances than that of SP3 and SP1 (Fig. 1C). Marker expression analysis showed higher expression of the two eMSC markers *PDGFRB* (CD140b) and *MCAM* (CD146) in SP3 and SP1 when compared to the other SPs (Supplementary Fig S1A, B). Interestingly, cells in SP3 and SP1 were mostly (99.8%) from the freshly isolated cells before culture, while cells in the other SPs were mostly (0.2%) from the sample after cultured for 14-day (Supplementary Fig S1C, D).

To investigate the differentiation relationship of the SPs, cell trajectory and pseudotime inference analysis was performed using Monocle 2 [30, 31]. The results revealed that the majority of the SP3 cells and a proportion of SP1 cells were located at the root, while majority of the SP0 and SP2 cells were distinctly at the terminals, consistent with their differentiation after culture (Fig. 1D, E). Cells along the trajectory were mostly from SP1 and SP4, indicating that they were intermediate cell types.

Based on single-cell sequencing, we selected LEPR and several other markers, and in preliminary experiments, we found that $LEPR^+$ eMSCs exhibited superior clonogenic potential compared to other marker-positive

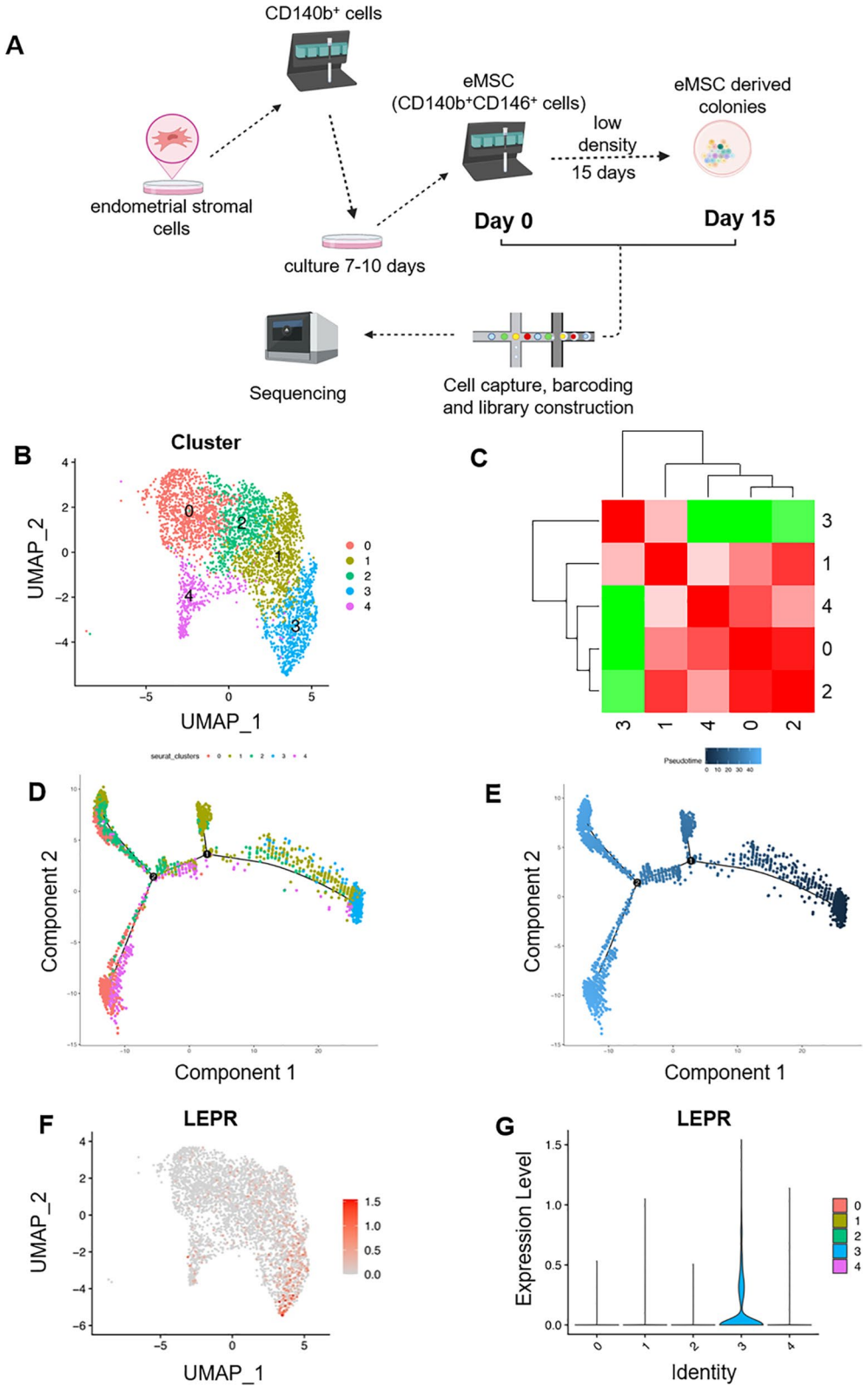

Fig. 1 A single-cell atlas of cultured human eMSCs. **A** Schematic of the study design. The image was created by BioRender (Fang, Y. (2026) https://BioRender.com/6b4epbq). **B** Unsupervised clustering of scRNA-seq data combining serial magnetic beaded eMSCs and 15-day single-cell cloning of eMSCs. **C** The heatmap showing the Pearson's correlation coefficient of 5 subpopulations. Developmental trajectories of 5 subpopulations colored by **D** clusters and **E** pseudotime. **F** Expression distribution of *LEPR* among clustering. **G** Violin plots showing *LEPR* among 5 subpopulations

populations. In mouse bone marrow MSCs, Lepr marks a quiescent, multipotent population crucial for hematopoiesis [32], suggesting that LEPR$^+$ eMSCs in humans may similarly possess enhanced regenerative and self-renewal capabilities. Notably, Lepr, which has been shown to be expressed by mouse bone marrow MSCs [32], was abundantly and specifically expressed in SP3 (Fig. 1F, G), with 29.33% of SP3 cells being LEPR$^+$. These findings collectively suggest that the eMSCs in SP3 represent a subset of primitive eMSCs. Base from our preliminary data and previous publications, we focused on the expression of LEPR$^+$ eMSCs.

LEPR$^+$ eMSCs in a single-cell dataset of primary human endometrium

To gain insight into human eMSCs in vivo, a scRNA-seq dataset of primary human endometrium [10] was analyzed. The dataset was derived from a total of 65,984 high-quality cells from endometrial biopsies at different phases of the menstrual cycle from 10 healthy donors with regular menstrual cycles and without gynecologic pathology. Nine distinct cell types were distinguished by specific biomarkers (Supplementary Table S7), namely NK cells, endothelia, lymphocytes, macrophages, perivascular cells, stromal fibroblasts, ciliated epithelia, glandular epithelia, and luminal epithelia (Fig. 2A).

In the dataset, 2,319 CD140b$^+$CD146$^+$ cells were identified. Clustering analysis of these primary human eMSCs revealed six distinct clusters, labeled C0 to C5, consisting of 1,149 cells (C0: 49.6%), 425 cells (C1: 18.3%), 325 cells (C2: 14.0%), 177 cells (C3: 7.6%), 124 cells (C4: 10.8%), and 119 cells (C5: 5.1%), respectively (Fig. 2B). The genes predominantly expressed in each cluster are shown in Fig. 2C. Specifically, *IGFBP1* and *IGF1* were prominently expressed in C0, *NOTCH3* and *RGS5* in C1, *ACTA2*, *MYH11*, and *JAG1* in C2, *MKI67*, *CENPF*, and *TOP2A* in C3, *LEPR* and *HES1* in C4, and *WFDC2* and *CLDN4* in C5 when compared to genes in the other clusters (Fig. 2C, D) of human endometrial cells. Based on the gene expression profile, C4 cluster contained as the LEPR$^+$ eMSC.

Relationship between cultured eMSCs and primary human endometrial cells

To investigate the relationship between cultured eMSCs and primary human endometrial cells, we integrated the above two single-cell datasets and corrected them for batch effects. Clustering analysis revealed 16 subpopulations in the combined dataset (Supplementary Fig S2A). To correlate the subpopulations (SP0-4) in the cultured eMSCs and the endometrial cell types in the primary human endometrial dataset, we mapped the identified cell types and subpopulations to the integrated dataset (Fig. 2A).

Our analysis revealed that SP0, SP2, and SP4 were more differentiated and were close together. Specifically, SP0 was adjacent to the ciliated epithelial cells and the endothelial cells, SP2 was distinct from other cell types but close to a small subpopulation of stromal cells, and SP4 was close to the ciliated epithelial cells. SP3 and SP1 were at the root of the in vitro differentiation trajectories of eMSCs. They formed a group distinct from the other three SPs. SP3 was between the perivascular cells and the bulk of stromal cells, while SP1 was near the bulk of stromal cells (Fig. 3A).

We further examined the gene expression of endometrial cell type-specific markers within the eMSC SPs. Besides the perivascular cell markers, stromal cell markers, and luminal epithelial cell markers, other cell-type markers were either expressed at low levels or not at all in the cultured eMSCs (Supplementary Fig S2C, D, E). The perivascular cell marker *PDGFRB* and the stromal cell marker *HAND2* were most abundantly expressed in SP3, while the luminal epithelial cell marker *MSX1* was mostly expressed in SP0 and SP2 (Supplementary Fig S2F, G, H). These observations suggested that the various eMSC SPs were related to certain primary endometrial cell types. Additionally, based on the highly variable features, we determined the correlation between the eMSCs in culture and those in the primary human endometrial tissue. Pearson correlation analysis revealed a high correlation between them (Supplementary Fig S2B), indicating that the cultured eMSCs shared similar characteristics with those derived from the human endometrium.

Cell fate trajectory analysis of cultured eMSCs and primary eMSCs

To investigate the transition of eMSCs to terminally differentiated endometrial cells at single-cell resolution, we performed cell fate trajectory and pseudotime analysis using Monocle 3 [33] on the integrated dataset, which includes both the cultured eMSCs and various endometrial cell types within the primary human endometrium.

Our trajectory analysis revealed a continuum of cells, with a 'root' primarily corresponding to the cultured eMSCs and a terminal population corresponding to luminal and glandular epithelia, and three distinct branch points (Fig. 3B, C). States 1 and 2 were predominantly composed of epithelial cells, including glandular, luminal, and ciliated types (Fig. 3B, D). State 3 consisted mainly of endothelial and stromal cells, which might represent an intermediate phase in eMSC differentiation (Fig. 3B - D). State 5 included cultured eMSCs along with some perivascular, stromal, and endothelial cells, which, based on pseudotime analysis, represented the initial stage of endometrial cell differentiation (Fig. 3B - D).

Notably, trajectory analysis revealed that the SP3 and SP0 subpopulations of cultured eMSCs were located at

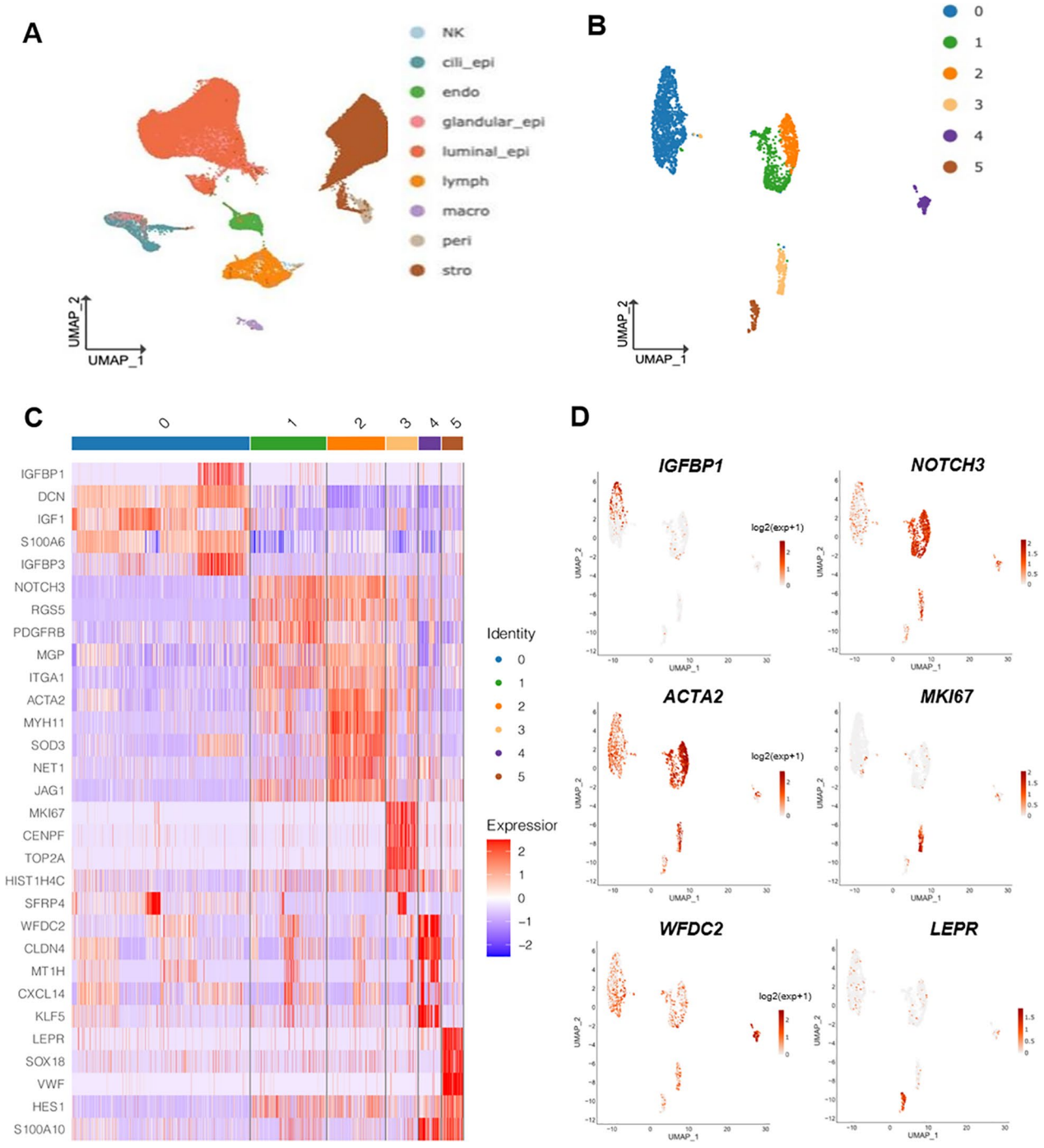

Fig. 2 A single-cell atlas of primary human eMSCs and their relationship to primary human endometrial cells. **A** Unsupervised clustering of scRNA-seq data of primary human endometrial cells from 10 donors. **B** Unsupervised clustering of scRNA-seq data of eMSCs of primary human endometrial cells. **C** The distinct expressed genes of different clusters of primary human eMSCs. **D** The distribution of *IGFBP1*, *NOTCH3*, *ACTA2*, *MKI67*, *LEPR* and *WFDC2* in primary human endometrial cells

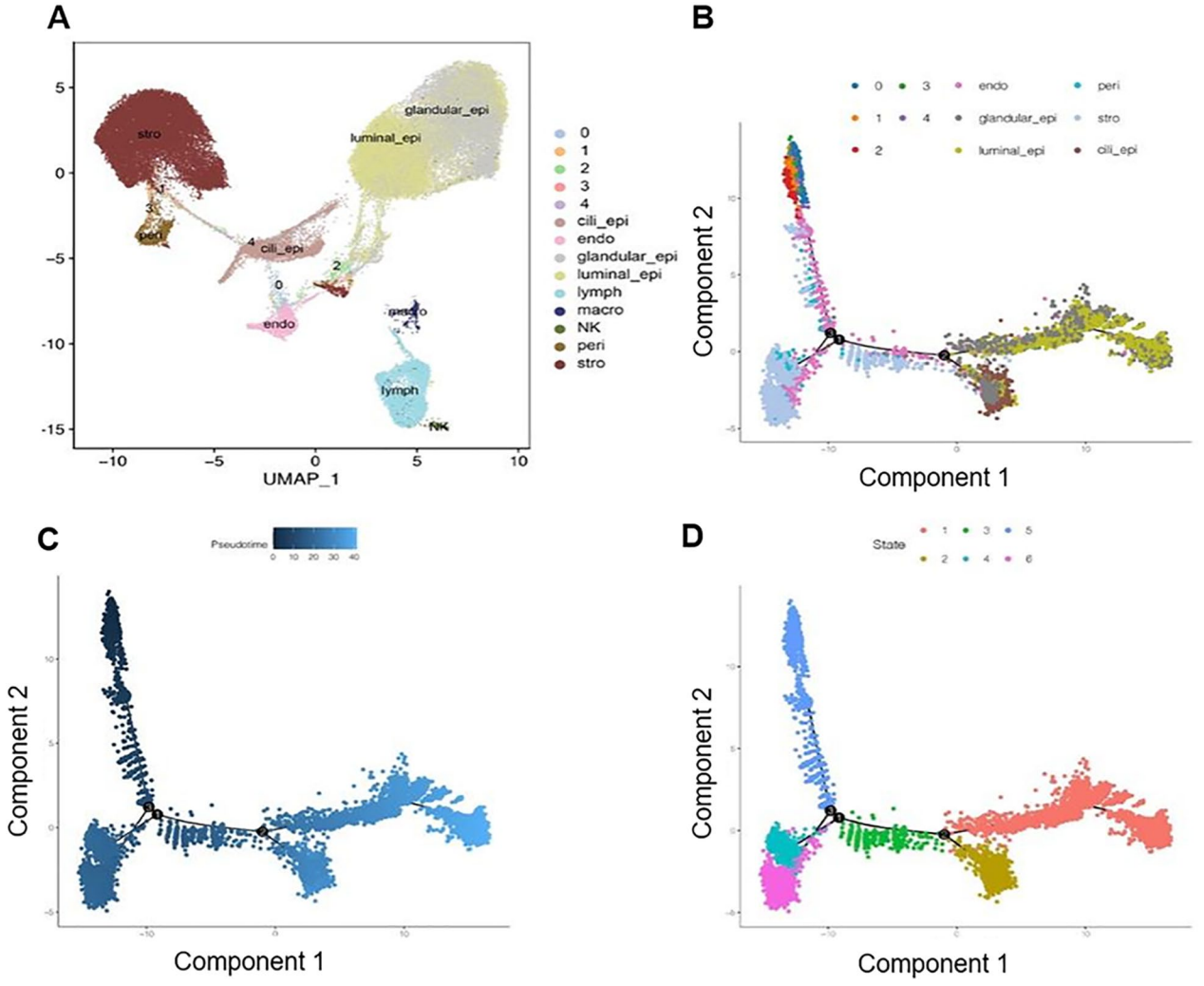

Fig. 3 A single-cell atlas of primary human eMSCs and their relationship to cultured eMSCs and primary human endometrial cells. **A** Unsupervised clustering of scRNA-seq data integrated primary human endometrial cells and cultured eMSCs. Developmental trajectories of 5 distinct subpopulations and various endometrial cell types, represented by **B** cluster classifications, **C** pseudotime dynamics, and **D** defined cellular states

the very beginning of the cell trajectory, suggesting that these subpopulations represented the most primitive state (Fig. 3B - D).

Human endometrium contains LEPR$^+$ eMSCs

The presence of LEPR$^+$ eMSCs in freshly isolated and cultured endometrial stromal cells was confirmed by flow cytometry. Figure 4A shows that 2.57 ± 1.51% of the unfractionated endometrial stromal cells expressed LEPR (n = 10), and the percentage increased to 12.03 ± 11.80% of the CD140b$^+$CD146$^+$ eMSCs (n = 10) from freshly isolated samples. Since LEPR expression changes across the menstrual cycle [34], we classified the eMSC samples into proliferative and secretory phase according to the histopathological results (Fig. 4B). The average expression of LEPR in the freshly isolated proliferative phase endometrial stromal cells was 2.24 ± 1.32%, while in the eMSC population, it was 12.26 ± 9.78% (n = 5, $P < 0.01$; Fig. 4B). The proportions were 2.90 ± 1.76% and 11.79 ± 14.75% for the secretory phase stromal cells and eMSCs, respectively (n = 7; Fig. 4B). The observations revealed that the proportion of eMSCs in the human endometrium remains unchanged.

Next, the effect of culture on the proportion of LEPR$^+$ eMSC was examined. The proportion of LEPR$^+$ cells was 25.59 ± 19.04% in the eMSC population and 2.61 ± 1.43% in the unfractionated stromal population (n = 12; Fig. 4C). In the proliferative phase samples (n = 5), the average proportions of LEPR$^+$ cells in the endometrial stromal cells and the eMSC populations were 2.43 ± 1.23% and 23.03 ± 18.51%, respectively (Fig. 4C). In the secretory phase samples (n = 7), the corresponding proportions were 2.75 ± 1.64% and 27.41 ± 20.66% (Fig. 4D). These findings demonstrated similar expression levels of LEPR in freshly isolated and cultured endometrial stromal cells.

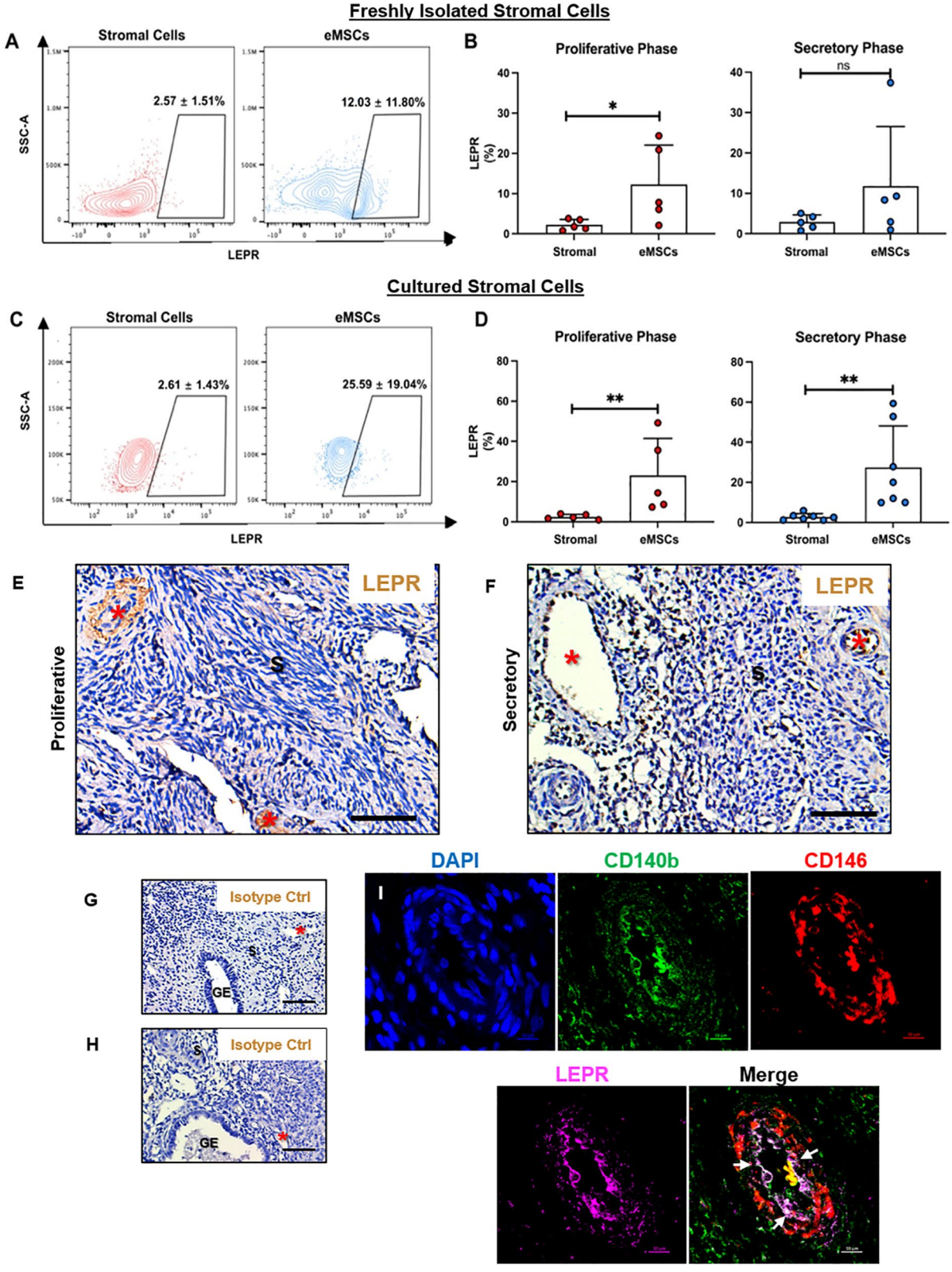

Fig. 4 (See legend on next page.)

(See figure on previous page.)

Fig. 4 The expression and location of leptin receptor (LEPR) in human endometrium and its relationship with endometrial mesenchymal stem cells (eMSCs). **A** Representative contour plots showing the expression of LEPR in freshly isolated endometrial stromal cells and eMSCs (n = 10). **B** The expression of LEPR at different menstrual phase of freshly isolated endometrial stromal cells and eMSCs (proliferative: n = 5; secretory: n = 5). **C** Representative contour plots showing the expression of LEPR in cultured endometrial stromal cells and eMSCs (n = 12). **D** The expression of LEPR in different menstrual phases of cultured endometrial stromal cells and eMSCs (proliferative: n = 5; secretory: n = 7). Full-thickness human endometrial sections immunohistochemical stained with LEPR from **E** proliferative and **F** secretory phase of the menstrual cycle. Isotype controls for **G** proliferative and **H** secretory sample, respectively. *, blood vessel; GE, glandular epithelium; S, stroma. (Scale bar: 50 μm). **I** Representative immunofluorescent images showing the co-localization (white arrows) of CD140b (green; pericytes), CD146 (red; endothelial) and LEPR (pink) in blood vessels in the endometrial stroma. (Scale bar: 10 μm). Results are presented as mean ± SD; **, P < 0 .01

LEPR$^+$ eMSCs are localized to the perivascular region of the human endometrium

Immunohistochemical analysis demonstrated that LEPR staining was predominantly localized to blood vessels within the endometrium (Fig. 4E, F). Glandular cells and myometrial cells also expressed LEPR. Co-localization of LEPR$^+$ staining with the CD140b$^+$CD146$^+$cells were observed around blood vessels in the human endometrium (Fig. 4I). Bioinformatic analysis of the composition LEPR$^+$ CD140b$^+$CD146$^+$ cells in the endometrium revealed that they consisted of 62.4% stromal cells, 30.1% perivascular cells, and 7.5% endothelial cells (Supplementary Fig S2A). Given that the perivascular cells include pericytes, adventitial fibroblasts, and mesenchymal stromal cells [35], there was likely significant overlap between the perivascular and the stromal cells within the LEPR$^+$ eMSC population. The CD140b$^+$CD146$^+$cells were negative for the endothelial marker CD31 [8], consistent with their identity as perivascular cells. CD140b is specifically expressed on perivascular cells and pericytes [36, 37]. There was a high level of co-expression of LEPR with CD140b around the blood vessels (Fig. 4I). Strong CD140b staining was also observed in most of the endometrial stromal cells, but not the endothelial or epithelial cells. CD146 was abundantly expressed in the endothelial cells and perivascular cells and less in pericytes as reported previously [38, 39].

LEPR$^+$ eMSCs exhibit high stem-cell characteristics

Flow cytometer sorted CD140b$^+$CD146$^+$cells but not CD140b$^-$CD146$^-$ cells exhibit MSC-like characteristics [8]. Therefore, the MSC attributes of cultured endometrial stromal cells from sorted eMSCs (CD140b$^+$CD146$^+$), LEPR$^+$ eMSCs (LEPR$^+$CD140b$^+$CD146$^+$) and LEPR$^-$ eMSCs (LEPR$^-$CD140b$^+$CD146$^+$) were compared. Significantly more colonies were generated by the LEPR$^+$ eMSCs than the eMSCs and the LEPR$^-$ eMSCs (P < 0.05, Fig. 5A). The colonies derived from the LEPR$^+$ eMSCs were larger in size comprising of densely packed cells (Fig. 5A). The cloning efficiencies of the LEPR$^+$ eMSCs, LEPR$^-$ eMSCs and eMSCs (n = 10) at passage 1 were 1.74 ± 2.05%, 1.19 ± 1.11% and 0.67 ± 0.56%, respectively (Fig. 5B). At passage 2, all the three groups formed more colonies (LEPR$^+$ eMSCs: 12.24 ± 7.60%; eMSCs: 4.68 ± 4.17% and LEPR$^-$ eMSCs: 4.16 ± 5.95%) and the number of colonies formed gradually declined with further passages. The difference in cloning efficiencies among the three groups was most significant in passage 4, when the eMSCs and the LEPR$^-$ eMSCs failed to form colonies (Fig. 5C). Overall, 7 out of 10 LEPR$^+$ eMSCs samples continued to be subcloned after passage 3. The results indicate that the LEPR$^+$ eMSCs possess better clonogenic and self-renewal ability.

Next, the multipotency of the three stromal subsets were assessed by in vitro differentiation assays (n = 4). For adipogenic lineage, the gene expression of *CEBPA* and *PPARG* were higher in the LEPR$^+$ eMSCs than eMSCs (Fig. 5D). The protein level of CEBPA was also found to be significantly higher in the LEPR$^+$ eMSCs (Fig. 5E). In addition, oil-red-O staining revealed the presence of adipocytes exclusively in the LEPR$^+$ eMSCs and eMSCs (Fig. 5F). The expression levels of osteogenic lineage-related genes at both mRNA (Supplementary Fig S3A) and protein levels (Supplementary Fig S3B, C) were similar among the three groups. For the chondrogenic lineage, LEPR$^+$ eMSCs exhibited higher levels of *COL10A1* expression compared to eMSCs (Supplementary Fig S3D). However, the difference in protein levels did not reach statistical significance (Supplementary Fig S3E, F). Overall, all three stromal subsets were able to differentiate into the three mesenchymal lineages.

LEPR$^+$ eMSCs exhibit quiescent properties

Mouse Lepr$^+$ MSCs are quiescent and activated upon injuries to form osteoblasts and adipocytes in bone marrow [40]. Since the endometrium is a highly dynamic tissue that undergoes cycles of proliferation, and differentiation, the cell cycle status of the LEPR$^+$ eMSCs was evaluated. We used the Seurat package to assign the cell cycle phases (G0/G1, G2M, S) in each SP in our scRNA-seq dataset (Supplementary Fig S1D) and found a high proportion (> 90%) of the cultured cells in the SP3 and SP4 subpopulation were at the G0/G1 phase (Supplementary Fig S4B). Due to the limitations of the Seurat package, it can only score and distinguish the G2M and S phases cells by specific markers, categorizing the remaining cells as being in the G0/G1 phase, thus mixing cells in the G0 and G1 phases. Quiescent cells typically express high levels of the cyclin-dependent kinase inhibitor p27 and low levels of the proliferation marker Ki67 [41, 42].

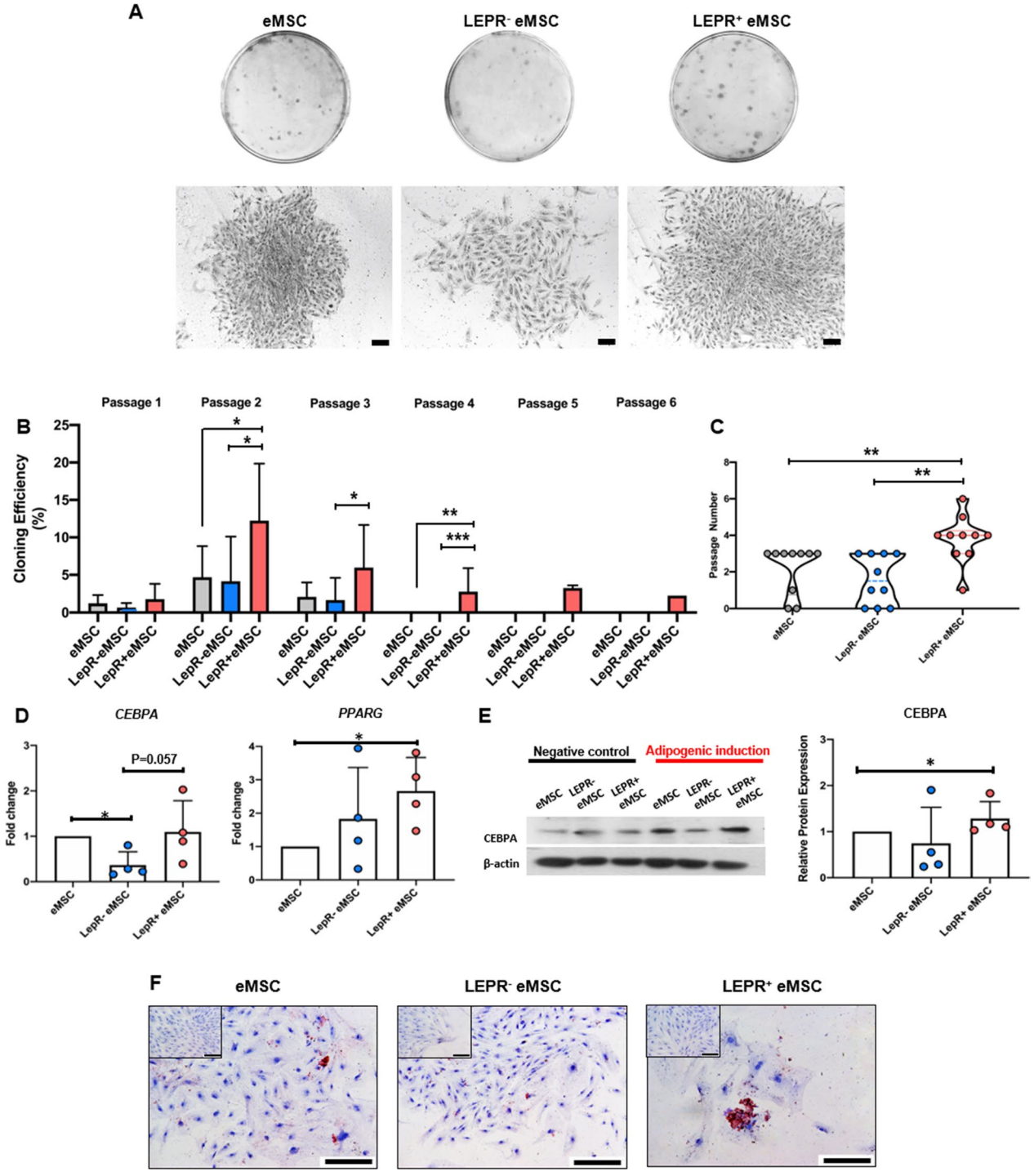

Fig. 5 Colony-forming activity and self-renewal ability of different cultured endometrial stromal subsets. **A** Representative image showing the distribution colonies and colony morphology in different subsets of cultured endometrial stromal cells after 15 days of culture (Scale bars = 200 μm). **B** The cloning efficiency of cultured endometrial stromal subsets at different cell passage (n = 10). **C** The self-renewal ability of different subsets of endometrial stromal cells in different generations after sorting (n = 10). In vitro differentiation potential of eMSCs, LEPR^{-} eMSCs and LEPR^{+} eMSCs into adipogenic lineage (n = 4). **D** Comparison of relative mRNA levels of adipogenic lineage-specific genes *CEBPA* and *PPARG*. **E** Representative western blot images and quantitative analysis of CEBPA protein. **F** Oil-red O staining (Scale bars: 100 μm). Results are presented as mean ± SD, * $P < 0.05$, ** $P < 0.01$

In our analysis, *CDKN1B* expression was highest in SP3 while *MKI67* expression was lowest (Supplementary Fig S4C, D). In primary eMSCs, clusters marked by *LEPR* also showed these characteristics (Supplementary Fig S4E—G), suggesting that the LEPR$^+$ eMSCs exhibited a quiescent phenotype.

Next, a flow-cytometry method was used to determine the proportion of G0 cells in the eMSCs. Figure 6A shows the average distribution of G0, G1 and S/G2/M cells in different subsets of isolated primary endometrial stromal cells (n = 10). The LEPR$^+$ eMSCs exhibited a significantly higher proportion of cells in the G0 phase when compared with the other two subsets (Fig. 6B); the proportion of G0 cells in the eMSCs, LEPR$^-$ eMSCs and LEPR$^+$ eMSCs were 29.72 ± 21.60%, 27.16 ± 20.69% and 50.62 ± 24.89% respectively.

Stem cell quiescence ensures prolonged maintenance of stem cells and regulates stem-cell-specific properties [43]. To gain further insight into the characteristics of the LEPR$^+$ eMSCs, we identified the DEGs between the LEPR$^-$ eMSCs and the LEPR$^+$ eMSCs and revealed an upregulation of quiescence-related genes, including *RB1*, *RBL2*, *CDKN1A*, *CDKN1B* and *E2F4*, in LEPR$^+$ eMSCs (Fig. 6C). Notably, the heightened expression of these genes, except the increased expression of *E2F4* which promotes cell proliferation, were associated with induction of cellular quiescence [19, 44]. Quantification of these gene expressions by qPCR in revealed a trend consistent with the single-cell analysis. Particularly, the expression of *RB1*, *RBL2*, and *CDKN1B* genes were significantly elevated in the LEPR$^+$ eMSCs compared to eMSCs ($P < 0.05$, Fig. 6D). The findings strongly affirmed that the LEPR$^+$ eMSCs exhibited quiescent cells characteristics.

LEPR$^+$ eMSCs are the most communicative subset among endometrial cells

Next, we investigated the cell–cell interactions between LEPR$^+$ eMSCs, LEPR$^-$ eMSCs, and non-eMSCs by analyzing their ligand-receptor relationships with all endometrial cells in the primary human endometrium dataset [45]. The number of ligand-receptor pairs and counts of interactions among LEPR$^+$ eMSCs, LEPR$^-$ eMSCs and non-eMSCs were quantified (Fig. 7A, B). The data indicated that the LEPR$^+$ eMSCs were the most communicative subset among the three cell populations, providing insights into the internal regulatory role of the LEPR$^+$ eMSCs. We also determined the ligand-receptor relationships (Fig. 7C). Ligands ubiquitously expressed in the LEPR$^+$ eMSCs included IGF1 (insulin-like growth factor 1), and JAG1, and the expressed receptor was mainly FLT1 (also known as VEGFR-1, vascular endothelial growth factor receptor 1), NRP1 (neuropilin 1), and CD44. IGF-1 is a master regulator of growth hormone [46], which enhances cell growth, migration, and viability [47–49]. JAG1 is involved in Notch signaling and regulates endometrial receptivity [50]. In the interaction network, the LEPR$^+$ eMSCs and the LEPR$^-$ eMSCs communicated most frequently, and the communication was mainly through Notch and Wnt signaling, especially via WNT4, WNT5A, and NOTCH3 (Fig. 7C).

Notch receptors are highly present in LEPR$^+$ eMSCs

As our bioinformatics analysis showed that Notch signaling was significantly expressed in the cell–cell communication network of LEPR$^+$ eMSCs and other subsets within the human endometrium. We hypothesized that activation of Notch signaling led to the quiescence of LEPR$^+$ eMSCs.

To test this, we initially evaluated the expression of Notch-related molecules across different subsets of primary human endometrium at the single-cell level. Interestingly, the *NOTCH1*, *NOTCH4*, and *HES1* expression were abundant in the LEPR$^+$ eMSCs compared to the stromal cells, eMSCs, and LEPR$^-$ eMSCs (Fig. 7D). To validate these bioinformatics findings, the expression of these Notch-related proteins was assayed with flow cytometry using freshly isolated endometrial stromal cells. NOTCH2 was included as the positive control. Specifically, in freshly isolated endometrial stromal cells, the proportion of HES1 (n = 8) was 6.82 ± 4.62% in the LEPR$^+$ eMSCs, while in the stromal cells, eMSCs, and LEPR$^-$ eMSCs, it was 0.38 ± 0.54%, 3.53 ± 2.43%, and 1.89 ± 1.73%, respectively. The proportion of NOTCH1 (n = 8) was 5.97 ± 3.05% in the LEPR$^+$ eMSCs, and 0.25 ± 0.22%, 2.39 ± 1.66%, and 3.11 ± 5.09%, in the stromal cells, eMSCs, and LEPR$^-$ eMSCs respectively. The proportion of NOTCH2 (n = 8) was 1.03 ± 3.91% in the LEPR$^+$ eMSCs, and 0.20 ± 0.25%, 1.46 ± 0.57%, and 1.11 ± 1.25% in the stromal cells, eMSCs, and LEPR$^-$ eMSCs, respectively. Lastly, the proportion of NOTCH4 (n = 8) was 6.66 ± 2.86% in the LEPR$^+$ eMSCs, and 0.71 ± 0.78%, 1.93 ± 1.18%, and 1.78 ± 1.50%, in the stromal cells, eMSCs, and LEPR$^-$ eMSCs, respectively (Fig. 7E). Overall, the LEPR$^+$ eMSC subset displayed significantly higher expression of Notch related proteins than the other three groups.

Activation of Notch maintained the phenotypic expression of LEPR$^+$ eMSCs

Our bioinformatics analysis showed that Notch signaling was significantly expressed in the cell–cell communication network of LEPR$^+$ eMSCs and other subsets within the human endometrium. Therefore, we next studied the activation of Notch signaling on LEPR$^+$ eMSCs. The proportion of LEPR expression in LEPR$^+$ eMSCs increased from 2.43 ± 1.42% to 24.20 ± 25.60% when cultured on JAG1-coated plate when compared

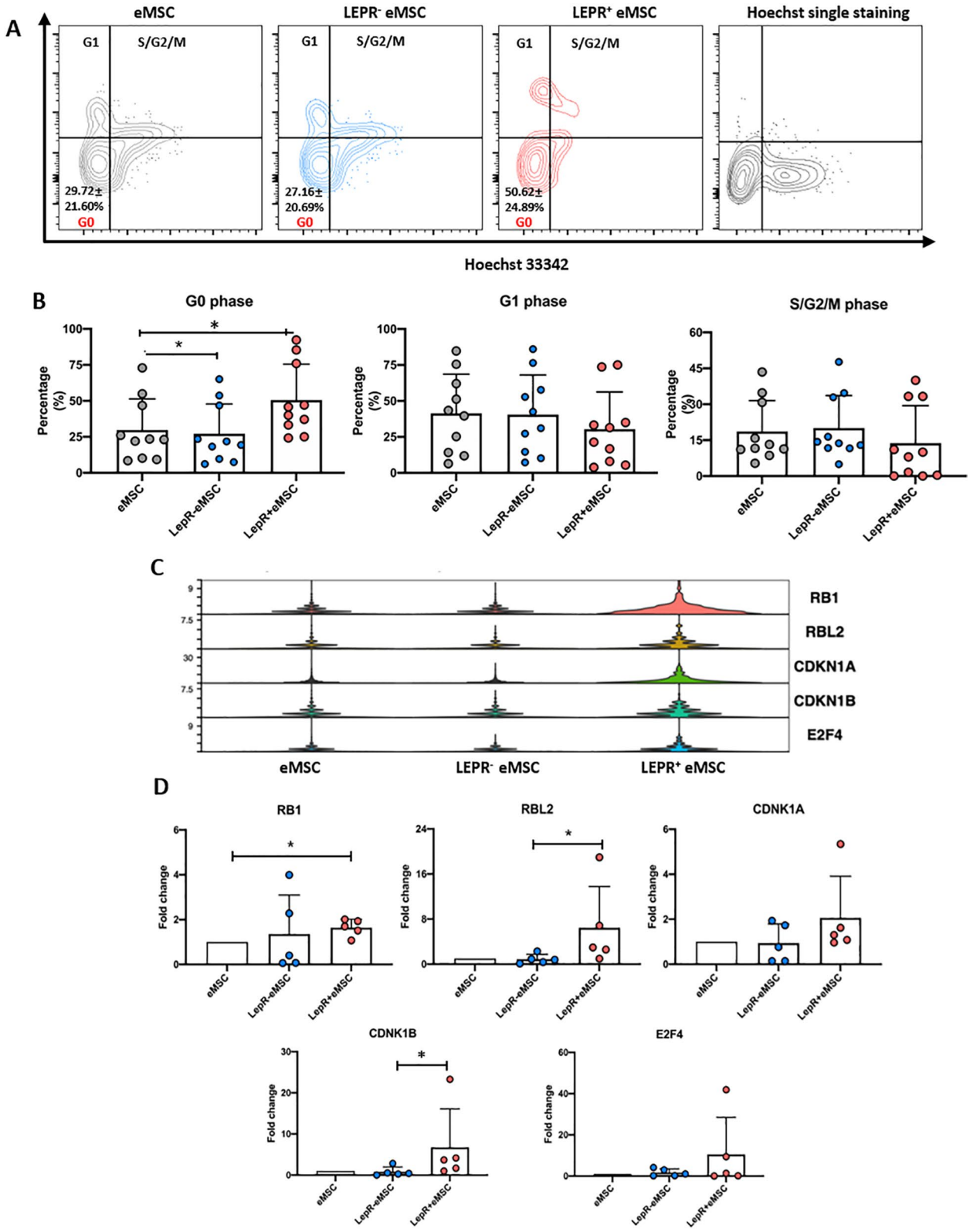

Fig. 6 The cell-cycle status of LEPR$^+$ eMSCs in freshly isolated endometrial stromal cells. **A** Representative contour plots for co-staining of Hoechst 33342 and Ki67 (n = 10). **B** The relative proportion of different freshly isolated endometrial stromal subsets in each cell cycle phase (n = 10). **C** Comparison of analysis of quiescent markers in different stromal subsets in the primary human endometrial single-cell dataset. **D** The qPCR results of quiescent markers in different stromal subsets derived from freshly isolated endometrial samples (n = 5). Results are presented as mean ± SD, * P < 0.05

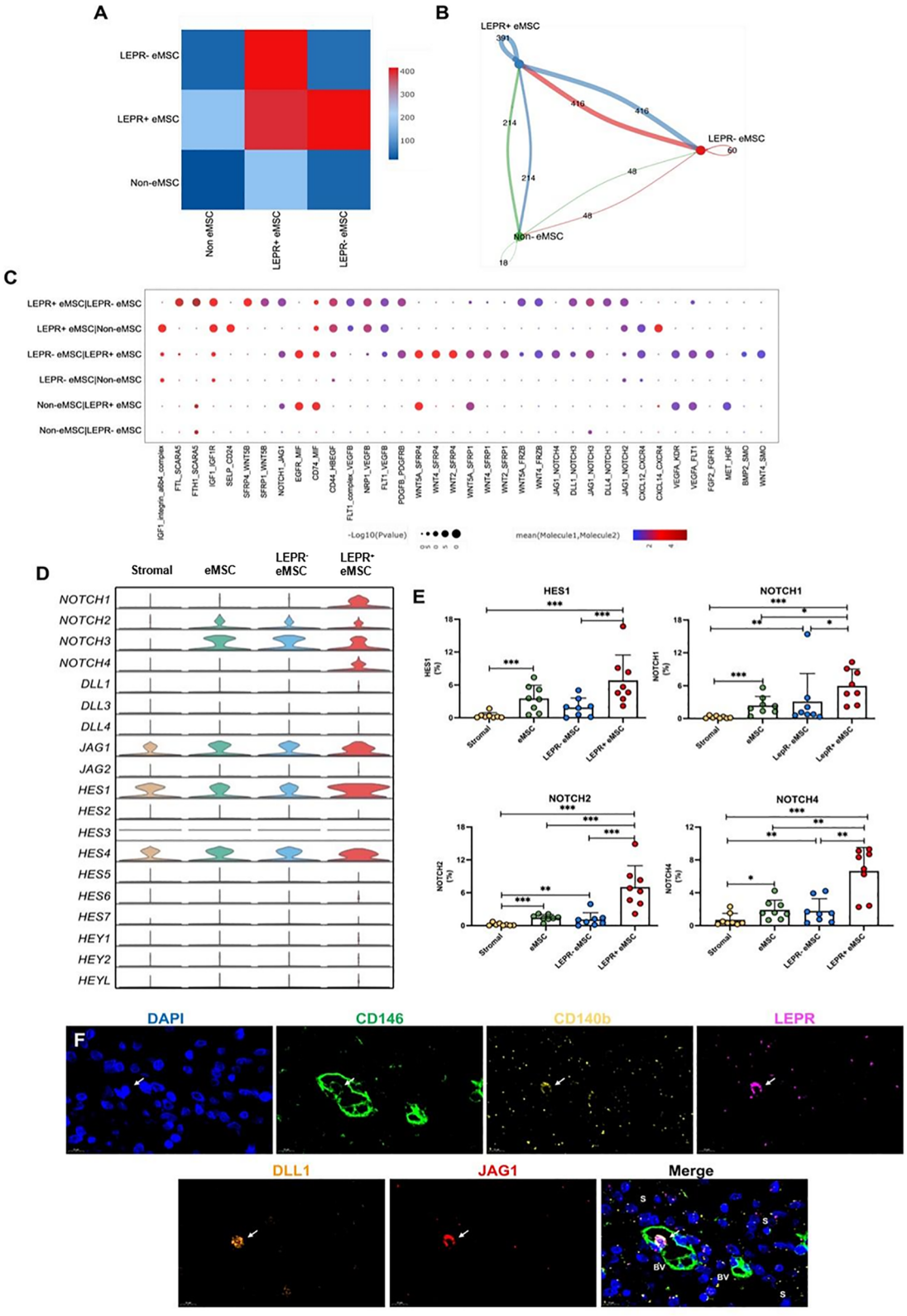

Fig. 7 (See legend on next page.)

(See figure on previous page.)

Fig. 7 The role and expression of Notch-related ligands and receptors in different endometrial stromal subsets. **A** Heatmap representation of the number of potential ligand-receptor pairs among different cell types of human endometrial cells. **B** The cell–cell interaction network was established by CellPhoneDB. **C** Ligand-receptor pairs of different cell types determined with CellPhoneDB are displayed with bubble plots. **D** The gene expression pattern of NOTCH-related molecules in stromal (yellow), eMSC (green), LEPR^{-} eMSC (blue), LEPR^{+} eMSC (red) from a primary human endometrial single-cell sequencing dataset (n = 10). **E** Quantification of HES1, NOTCH1, NOTCH2, and NOTCH4 in freshly isolated human endometrial stromal subsets (n = 8). Representative immunofluorescent images showing the co-localization (white arrows) of CD146 (green), CD140b (yellow), LEPR (pink), DLL1(orange) and JAG1(red) in blood vessels in the endometrial stroma. S, stroma; BV, blood vessels (Scale bar: 20 μm). The results are presented as the mean ± SD, * $P < 0.05$, ** $P < 0.01$, *** $P < 0.001$

to CTRL (Supplementary Fig S5A, B). Additionally, the proportion of eMSCs and LEPR^{+} eMSCs increased from 3.07 ± 2.42% to 7.89 ± 3.05% (Supplementary Fig S5C, D) and 0.20 ± 0.15% to 2.07 ± 1.14% (Supplementary Fig S5E, F), respectively. The above results demonstrate that Notch signaling also promotes the LEPR^{+} phenotype.

Furthermore, to assess the broader implications of Notch activation, we evaluated the impact on cell viability through a cell apoptosis assay. The cell viability of this model was studied with the cell apoptosis assay. The proportions of early apoptosis in the CTRL and JAG1-coated plates were 3.64 ± 0.92% and 4.81 ± 0.15%, respectively, while the proportions of late apoptosis were 2.41 ± 1.24% and 4.34 ± 2.81%, respectively (Supplementary Fig S5G). There was no significant difference in the comparison of early apoptosis (Supplementary Fig S5G and H, $P = 0.17$) and late apoptosis (Supplementary Fig S5G and I, $P = 0.34$) between the control and JAG1-coated group. The findings suggest that activation of the Notch pathway does not impact the cell's viability.

Localized co-expression of JAG1 and DLL1 in LEPR^{+} eMSCs

Since high expression of Notch receptors were detected on the LEPR^{+} eMSCs, we postulated that Notch ligands derived from neighboring cells in the endometrium could activate the Notch signaling pathway for stem cell quiescence. To investigate this, we examined the expression of Notch ligands across various endometrial cell types at single-cell level. The analysis revealed JAG1 was highly expressed in several cell types, including endothelial cells, perivascular cells, and epithelial cells during both the proliferative and the secretory phases (Supplementary Fig S4H, I). Additionally, there was lower expression levels of DLL1 in endothelial cells and NK cells during the secretory phase compared to the proliferative phase. A constant low expression of the other Notch ligands was detected across the menstrual cycle (Supplementary Fig S4H, I).

To investigate the spatial distribution of JAG1 and DLL1 within the endometrium and their potential association with LEPR^{+} eMSCs, multiplex immunohistochemistry was performed. The analysis revealed that JAG1 and DLL1 co-localized with a subset of LEPR^{+} eMSCs (Fig. 7F). Since co-localization was not observed in all LEPR^{+} eMSCs, this suggested heterogeneity in their interaction with these Notch ligands. In addition, expression of these ligands was observed in other endometrial cell types, though further analysis would be required to fully characterize their distribution across the various cell populations.

Discussion

Stem/progenitor cells in the endometrium are responsible for the cyclical proliferation, differentiation and regeneration of the tissue. The identification of stem cell markers can assist researchers in isolating these rare cells for in vitro studies. To date, there are two sets of well-characterized markers for human eMSCs, the co-expression of CD140b^{+}CD146^{+} [8] and the single marker sushi domain containing-2^{+} (SUSD2) [51] cells. However, one major obstacle is the heterogeneity within the eMSC population, i.e. the cells show cell-to-cell variability in phenotypic expression, proliferation capacity, and cytokine secretion [52].

The main finding of this study was the identification of the LEPR^{+} subpopulation within eMSCs. Compared with the negative subset, the LEPR^{+} eMSCs exhibited remarkably higher clonogenic activity at each passage, a better self-renewal ability, and comprised of more quiescent cells. This is the first study in which LEPR was characterized in endometrial stem cells, and our findings demonstrated that the endometrial LEPR^{+} subset possessed similar characteristics as the Lepr^{+} stromal cells in the bone marrow [40].

Human CD140b^{+}CD146^{+} eMSCs is a heterogeneous cell population [12]. In this study, scRNA-seq was performed on magnetic bead selected eMSCs and clonally derived eMSCs obtained from a secretory phase endometrial sample to better understand the differentiation trajectories of eMSCs during in vitro culture. A total of 5 subpopulations (SPs) were identified through unsupervised clustering. SP3, which largely stands at the root of differentiation trajectories, was considered the origin of the trajectory reconstruction. The distinct expression of LEPR in SP3 highly suggests that these cells play a critical role in stem cell regulation. Consistently, we identified 6 clusters in the primary eMSCs predominantly expressed *LEPR* in a primary human endometrial single-cell dataset [10]. Thus, both in vitro and in vivo data indicated *LEPR* marks a subset within eMSCs.

By integrating two single-cell datasets to elucidate the relationship between cultured eMSCs and endometrial

cells, we showed that SP1 and SP3 at the root of the differentiation trajectory were originated from undifferentiated eMSCs closely associated with stromal and perivascular cells. In contrast, SP0, SP2, and SP4 at the branches of the differentiation trajectory were derived from differentiated eMSCs more closely linked to epithelial cells, endothelial cells, and other unidentified cell types. These results indicate that the cultured eMSCs follow distinct differentiation pathways with specific subpopulations associated with various endometrial cell types.

Furthermore, Pearson correlation analysis revealed a significant correlation between the LEPR$^+$ eMSCs from the cultured eMSC dataset and the primary human endometrium, suggesting that LEPR$^+$ eMSCs maintained consistent properties both in vivo and in vitro. This highlights that the unique combination of LEPR, CD146, and CD140b as surface markers can be used to isolate primitive eMSCs from stromal cells in future experiments.

Lepr has been well studied in the mouse bone marrow [40, 53]. Lepr marks an adult bone marrow mesenchymal stromal cell population that accounts for 94% of the bone marrow colony forming unit fibroblasts [40]. Furthermore, Lepr$^+$ perivascular stromal cells in the bone marrow can secrete stem cell factor and CXCL12 to maintain and regulate murine hematopoiesis [54]. Lepr is also a marker for functional long-term hematopoietic stem cells (HSC) highly enriched in engrafting cells with embryonic-like transcriptomic properties [55]. In the gut, Lepr$^+$ mesenchymal cells can sense diet alterations and regulate the proliferation of mouse intestinal stem/progenitor cells [56]. It also plays an important role in colorectal carcinogenesis by proliferation to generate CD146$^+$ cancer-associated fibroblasts, thereby shaping the pro-tumor immune microenvironment [57].

Studies of LEPR in the endometrium remain limited and mainly focus on gynecological diseases such as endometriosis [58–60] and endometrial cancer [61, 62]. Several studies have shown a change in LEPR expression throughout the menstrual cycle [63]. Specifically, the LEPR expression levels are low in the early proliferative phase and peak in the early secretory phase [34]. In vivo, the LEPR expression is highly dependent on the estrogen receptor and progesterone receptor status in the endometrium [64]. A clinical study revealed that the expression of LEPR in the endometrium was significantly lower in the infertile women than the fertile women [65]. These observations hint at a potential relationship between LEPR, human endometrial and mesenchymal stem cells, and our study provides compelling evidence to support this association.

Although the expression level of LEPR is relatively low within the endometrial stromal compartment, it is more prominent within the CD140b$^+$CD146$^+$eMSC population. We found widespread expression of LEPR in the human endometrium, particularly concentrated around the blood vessels of the basalis region. The co-localization of LEPR and CD140b expressions along the blood vessels emphasized their correlation. Bioinformatics analysis indicated that the LEPR$^+$ eMSCs consisted of roughly 2/3 of stromal cells and 1/3 perivascular cells. Immunofluorescence results demonstrated that the majority of the LEPR$^+$ eMSCs were located around blood vessels. In the same experimental setting, the LEPR$^+$ eMSCs exhibited superior colony formation capabilities in terms of colony quantity and size, survival in subcloning conditions and differentiation ability towards the adipogenic lineage compared to eMSCs and LEPR$^-$ eMSCs. The better adipogenic lineage differentiation ability was not surprising because leptin, a hormone primarily derived from adipose tissue, acts through LEPR [66]. Another well-characterized marker for human eMSC is SUSD2 [51]. Since SUSD2$^+$ and CD140b$^+$CD146$^+$ eMSC reside in the perivascular niche, it will be worth investigating the role of LEPR on SUSD2$^+$ eMSCs in future studies.

Initially, we assumed that the LEPR$^+$ eMSCs were more proliferative based on their higher colony-forming ability. However, the cell cycle analyses based on bioinformatics analysis and in vitro experiments demonstrated that the LEPR$^+$ eMSCs possessed a higher proportion of cells in the G0 phase, i.e. the LEPR$^+$ eMSCs were more quiescent. In vivo, LEPR$^+$ eMSC are quiescent when residing in the niche. However, when cultured without the presence of specific growth factors or niche components, these LEPR$^+$ eMSC will undergo proliferation and differentiation as observed by the high clonogenic activity in vitro. Quiescent adult stem cells can be found in a variety of tissues, but their proportion is more prevalent in low-turnover tissues such as skeletal muscle or the brain [67]. The hematopoietic system remains an exception among the high turnover 'tissue'. HSCs mostly remain quiescent and give rise to multipotent progenies to maintain hematopoiesis during normal homeostasis [68–70]. Our findings revealed a small population of quiescent stem cells existed in a high turnover tissue—the endometrium. The rarity of the LEPR$^+$ eMSCs (approximately 0.1% of human endometrial stromal cells) will be a challenge for in-depth evaluation of the quiescent cell state likely to be involved in the periodic regeneration of the human endometrium. Future studies should investigate the loss of LEPR during endometrial regeneration and identify key regulators maintaining the LEPR$^+$ eMSC quiescent in vivo.

Interestingly, we found that the LEPR$^+$ eMSCs express several Notch receptors at high levels. Notch signaling is essential for maintaining stem cell quiescence [71, 72]. Certain Notch receptors and their ligands play pivotal roles in regulating specific hematopoietic progenitor subsets within distinct marrow microenvironments [73,

74]. We hypothesize that niche cells surrounding LEPR$^+$ eMSCs express Notch ligands, which activate Notch signaling in the LEPR$^+$ eMSCs. The loss of these niche cells may activate the LEPR$^+$ eMSCs. Our single-cell analysis revealed JAG1 and DLL1 exhibit high expression levels when compared to other Notch ligands in various types of endometrial cells. Previous studies have demonstrated the critical role of Notch ligands in regulating stem cells across multiple systems including the endometrium [75–78]. For example, after osteoblast ablation, the loss of JAG1-mediated signaling disrupts HSC quiescence [79]. The transcription factor Pax7 is as a marker of quiescent MuSCs [80, 81]. MuRCs (muscle reserve cells) with high Pax7 expression (Pax7^{High}) are closely associated with JAG1 and other Notch signaling components for maintaining their deep quiescent state, while Pax7^{Low} MuRCs display an increased tendency toward myogenic differentiation [82]. DLL1 is a crucial Notch ligand for maintaining quiescence of neural stem cells in the adult mouse subventricular zone [83]. DLL1-mediated Notch signaling is also indispensable in the MuSCs, where it significantly enhances Pax7 expression (84). Our group has previously demonstrated that Notch1 mediates the quiescence-promoting effects of JAG1 in eMSCs [78]. Here, both JAG1 and DLL1 co-localized with LEPR$^+$ eMSCs, suggesting their involvement in regulating endometrial stem cell behavior and maintenance of quiescence. In future, it will worth investigating the action of Notch on the cell cycle of LEPR$^+$ eMSCs. It is likely these cells will be in a quiescent state upon Notch activation. The reversible state of quiescence is important for the long-term maintenance of stem cell system of stromal cells. In a dynamic tissue such as the endometrium, quiescence can preserve their self-renewal capacity for tissue regeneration.

Conclusion

In this study, we identified a novel LEPR$^+$ subpopulation within human endometrial mesenchymal stem cells (eMSCs), characterized by enhanced clonogenicity, quiescence, and distinct gene expression patterns. Integrative single-cell transcriptomic analysis of cultured and primary human endometrial tissues demonstrated that LEPR$^+$ eMSCs represent a primitive, quiescent subset enriched for Notch receptor expression. Functional assays confirmed their superior stemness and potential for endometrial regeneration. Our findings indicate that Notch signaling, particularly mediated by JAG1 and DLL1, plays a critical role in maintaining the quiescent state of LEPR$^+$ eMSCs. These results advance the understanding of human endometrial stem cell biology and provide a foundation for future therapeutic applications targeting regenerative disorders of the endometrium.

Abbreviations

eMSCs	Endometrial mesenchymal stem cells
LEPR	Leptin receptor
scRNA-seq	Single-cell RNA sequencing
UMI	Unique molecular identifier
UMAP	Uniform Manifold Approximation and Projection
PBS	Phosphate-buffered saline
FACS	Fluorescence-activated cell sorting
DAPI	4′,6-Diamidino-2-phenylindole
qPCR	Quantitative polymerase chain reaction
RT-PCR	Reverse transcription polymerase chain reaction
GM	Growth medium
HES1	Hairy and enhancer of split-1 (Notch target gene)
JAG1	Jagged 1 (Notch ligand)
DLL1	Delta-like ligand 1
CD	Cluster of differentiation (e.g., CD140b = PDGFRβ)
Notch	Neurogenic locus notch homolog protein

Supplementary Information

The online version contains supplementary material available at https://doi.org/10.1186/s13287-025-04803-7.

Supplementary Material 1.

Supplementary Material 2.

Supplementary Material 3.

Supplementary Material 4.

Supplementary Material 5.

Supplementary Material 6.

Supplementary Material 7.

Supplementary Material 8.

Supplementary Material 9.

Acknowledgements

We sincerely thank all participants who donated endometrial tissue for this study. We acknowledge the assistance of research nurse Joyce Yuen and the gynecology teams at Queen Mary Hospital and The University of Hong Kong Shenzhen Hospital for sample collection. Technical support from the staff at the Centre for PanorOmic Sciences, Imaging and Flow Cytometry Core, and the Centre of Comparative Medicine Research at The University of Hong Kong is gratefully acknowledged. The authors declare that they have not used AI-generated work in this manuscript.

Author contributions

Yuan Fang, Dandan Cao, William S.B. Yeung, and Rachel W.S. Chan conceptualized and designed the study. Yuan Fang conducted the experiments and data analysis. Yuan Fang, Dandan Cao, Cheuk-Lun Lee, Philip C.N. Chiu, Ernest H.Y. Ng, and Rachel W.S. Chan drafted the manuscript. William S.B. Yeung and Rachel W.S. Chan reviewed and edited the manuscript. All authors read and approved the final manuscript.

Funding

This study was supported by the National Natural Science Foundation of China/Research Grants Council Joint Research Scheme (N_HKU 732/20), the Sanming Project of Medicine in Shenzhen, China (SZSM201612083), Guangdong Basic and Applied Basic Research Foundation, China (2023A1515220177) and the Research Grants Council General Research Fund (17115320).

Data availability

The single-cell RNA-seq datasets analyzed in this study include a publicly available dataset (GSE111976) and newly generated data. The newly generated raw and processed data will be made publicly available in an appropriate repository upon publication.

Declarations

Ethics approval and consent to participate
This study was approved by the Institutional Review Board of The University of Hong Kong/Hospital Authority Hong Kong West Cluster (Approval No. UW20-465, approved on 22 June 2020, Title: Reconstruction of endometrial-like tissue from human endometrial stem cells) and the Institutional Review Board of the University of Hong Kong-Shenzhen Hospital (Approval No. [2018]94, approved on 13 September 2018, Title: Culture and expansion of endometrial stem cells for autologous transplantation in the treatment of infertility). Written informed consent was obtained from all participants prior to sample collection.

Consent for publication
Not applicable.

Competing interests
The authors declare that they have no competing interests.

Received: 21 April 2025 / Accepted: 4 November 2025
Published online: 23 December 2025

References

1. Wagers AJ, Weissman IL. Plasticity of adult stem cells. Cell. 2004;116(5):639–48.
2. Poulsom R, Alison MR, Forbes SJ, Wright NA. Adult stem cell plasticity. J Pathol. 2002;197(4):441–56.
3. Tang DG. Understanding cancer stem cell heterogeneity and plasticity. Cell Res. 2012;22(3):457–72.
4. Greulich P, Simons BD. Dynamic heterogeneity as a strategy of stem cell self-renewal. Proc Natl Acad Sci. 2016;113(27):7509–14.
5. Kong Y, Shao Y, Ren C, Yang G. Endometrial stem/progenitor cells and their roles in immunity, clinical application, and endometriosis. Stem Cell Res Ther. 2021;12:1–16.
6. Gargett CE, Schwab KE, Deane JA. Endometrial stem/progenitor cells: the first 10 years. Hum Reprod Update. 2016;22(2):137–63.
7. Cousins FL, Filby CE, Gargett CE. Endometrial stem/progenitor cells–their role in endometrial repair and regeneration. Front Reprod Health. 2022;3:811537.
8. Schwab KE, Gargett CE. Co-expression of two perivascular cell markers isolates mesenchymal stem-like cells from human endometrium. Hum Reprod. 2007;22(11):2903–11.
9. Xu S, Chan RW, Ng EH, Yeung WS. Spatial and temporal characterization of endometrial mesenchymal stem-like cells activity during the menstrual cycle. Exp Cell Res. 2017;350(1):184–9.
10. Wang W, Vilella F, Alama P, Moreno I, Mignardi M, Isakova A, et al. Single-cell transcriptomic atlas of the human endometrium during the menstrual cycle. Nat Med. 2020;26(10):1644–53.
11. Garcia-Alonso L, Handfield L-F, Roberts K, Nikolakopoulou K, Fernando RC, Gardner L, et al. Mapping the temporal and spatial dynamics of the human endometrium in vivo and in vitro. Nat Genet. 2021;53(12):1698–711.
12. Cao D, Chan RW, Ng EH, Gemzell-Danielsson K, Yeung WS. Single-cell RNA sequencing of cultured human endometrial CD140b+ CD146+ perivascular cells highlights the importance of in vivo microenvironment. Stem Cell Res Ther. 2021;12(1):1–15.
13. Hedlund E, Deng Q. Single-cell RNA sequencing: technical advancements and biological applications. Mol Aspects Med. 2018;59:36–46.
14. Hwang B, Lee JH, Bang D. Single-cell RNA sequencing technologies and bioinformatics pipelines. Exp Mol Med. 2018;50(8):1–14.
15. Wen L, Tang F. Single-cell sequencing in stem cell biology. Genome Biol. 2016;17(1):1–12.
16. Potter SS. Single-cell RNA sequencing for the study of development, physiology and disease. Nat Rev Nephrol. 2018;14(8):479–92.
17. Luo M, Li J-F, Yang Q, Zhang K, Wang Z-W, Zheng S, et al. Stem cell quiescence and its clinical relevance. World J Stem Cells. 2020;12(11):1307.
18. Cho IJ, Lui PP, Obajdin J, Riccio F, Stroukov W, Willis TL, et al. Mechanisms, hallmarks, and implications of stem cell quiescence. Stem Cell Reports. 2019;12(6):1190–200.
19. Cheung TH, Rando TA. Molecular regulation of stem cell quiescence. Nat Rev Mol Cell Biol. 2013;14(6):329–40.
20. Artavanis-Tsakonas S, Muskavitch MA. Notch: the past, the present, and the future. Curr Top Dev Biol. 2010;92:1–29.
21. Chiba S. Concise review: Notch signaling in stem cell systems. Stem Cells. 2006;24(11):2437–47.
22. Bjornson CR, Cheung TH, Liu L, Tripathi PV, Steeper KM, Rando TA. Notch signaling is necessary to maintain quiescence in adult muscle stem cells. Stem Cells. 2012;30(2):232–42.
23. Zhang S, Chan RWS, Ng EHY, Yeung WSB. The role of Notch signaling in endometrial mesenchymal stromal/stem-like cells maintenance. Commun Biol. 2022;5(1):1064.
24. Hao Y, Hao S, Andersen-Nissen E, Mauck WM, Zheng S, Butler A, et al. Integrated analysis of multimodal single-cell data. Cell. 2021;184(13):3573–87.
25. Korsunsky I, Millard N, Fan J, Slowikowski K, Zhang F, Wei K, et al. Fast, sensitive and accurate integration of single-cell data with harmony. Nat Methods. 2019;16(12):1289–96.
26. Yu G, Wang L-G, Han Y, He Q-Y. ClusterProfiler: an R package for comparing biological themes among gene clusters. OMICS. 2012;16(5):284–7.
27. Efremova M, Vento-Tormo M, Teichmann SA, Vento-Tormo R. Cell PhoneDB: inferring cell–cell communication from combined expression of multi-subunit ligand–receptor complexes. Nat Protoc. 2020;15(4):1484–506.
28. Cao J, Spielmann M, Qiu X, Huang X, Ibrahim DM, Hill AJ, et al. The single-cell transcriptional landscape of mammalian organogenesis. Nature. 2019;566(7745):496–502.
29. Cao M, Chan RW, Cheng FH, Li J, Li T, Pang RT, et al. Myometrial cells stimulate self-renewal of endometrial mesenchymal stem-like cells through WNT5A/β-catenin signaling. Stem Cells. 2019;37(11):1455–66.
30. Qiu X, Hill A, Packer J, Lin D, Ma Y-A, Trapnell C. Single-cell mRNA quantification and differential analysis with Census. Nat Methods. 2017;14(3):309–15.
31. Qiu X, Mao Q, Tang Y, Wang L, Chawla R, Pliner HA, et al. Reversed graph embedding resolves complex single-cell trajectories. Nat Methods. 2017;14(10):979–82.
32. Yue R, Zhou BO, Shimada IS, Zhao Z, Morrison SJ. Leptin receptor promotes adipogenesis and reduces osteogenesis by regulating mesenchymal stromal cells in adult bone marrow. Cell Stem Cell. 2016;18(6):782–96.
33. Cao J, Spielmann M, Qiu X, Huang X, Ibrahim DM, Hill AJ, et al. The single-cell transcriptional landscape of mammalian organogenesis. Nature. 2019;566(7745):496–502.
34. González RnR, Caballero-Campo P, Jasper M, Mercader A, Devoto L, Pellicer A, et al. Leptin and leptin receptor are expressed in the human endometrium and endometrial leptin secretion is regulated by the human blastocyst. The Journal of Clinical Endocrinology & Metabolism. 2000; 85(12): 4883–8.
35. Benabid A, Peduto L. Mesenchymal perivascular cells in immunity and disease. Curr Opin Immunol. 2020;64:50–5.
36. Song S, Ewald AJ, Stallcup W, Werb Z, Bergers G. PDGFRβ+ perivascular progenitor cells in tumours regulate pericyte differentiation and vascular survival. Nat Cell Biol. 2005;7(9):870–9.
37. Hellström M, Kalén M, Lindahl P, Abramsson A, Betsholtz C. Role of PDGF-B and PDGFR-β in recruitment of vascular smooth muscle cells and pericytes during embryonic blood vessel formation in the mouse. Development. 1999;126(14):3047–55.
38. Corselli M, Chin CJ, Parekh C, Sahaghian A, Wang W, Ge S, et al. Perivascular support of human hematopoietic stem/progenitor cells. Blood. 2013;121(15):2891–901.
39. Bardin N, Moal V, Anfosso F, Daniel L, Brunet P, Sampol J, et al. Soluble CD146, a novel endothelial marker, is increased in physiopathological settings linked to endothelial junctional alteration. Thromb Haemost. 2003;90(11):915–20.
40. Zhou BO, Yue R, Murphy MM, Peyer JG, Morrison SJ. Leptin-receptor-expressing mesenchymal stromal cells represent the main source of bone formed by adult bone marrow. Cell Stem Cell. 2014;15(2):154–68.
41. Lindell E, Zhong L, Zhang X. Quiescent cancer cells—a potential therapeutic target to overcome tumor resistance and relapse. Int J Mol Sci. 2023;24(4):3762.
42. La T, Chen S, Guo T, Zhao XH, Teng L, Li D, et al. Visualization of endogenous p27 and Ki67 reveals the importance of a c-Myc-driven metabolic switch in promoting survival of quiescent cancer cells. Theranostics. 2021;11(19):9605.
43. Mohammad K, Dakik P, Medkour Y, Mitrofanova D, Titorenko VI. Quiescence entry, maintenance, and exit in adult stem cells. Int J Mol Sci. 2019;20(9):2158.
44. Rumman M, Dhawan J, Kassem M. Concise review: quiescence in adult stem cells: biological significance and relevance to tissue regeneration. Stem Cells. 2015;33(10):2903–12.
45. Wang W, Vilella F, Alama P, Moreno I, Mignardi M, Isakova A, et al. Single-cell transcriptomic atlas of the human endometrium during the menstrual cycle. Nat Med. 2020;26(10):1644–53.

46. Clemmons DR, Snyder P, Martin K. Physiology of insulin-like growth factor 1. Up To Date Website. 2014.
47. Ferreira-Mendes JM, de Faro Valverde L, Torres Andion Vidal M, Paredes BD, Coelho P, Allahdadi KJ, et al. Effects of IGF-1 on proliferation, angiogenesis, tumor stem cell populations and activation of AKT and hedgehog pathways in oral squamous cell carcinoma. International Journal of Molecular Sciences. 2020; 21(18): 6487.
48. Huat TJ, Khan AA, Pati S, Mustafa Z, Abdullah JM, Jaafar H. IGF-1 enhances cell proliferation and survival during early differentiation of mesenchymal stem cells to neural progenitor-like cells. BMC Neurosci. 2014;15(1):1–13.
49. Lin M, Liu X, Zheng H, Huang X, Wu Y, Huang A, et al. IGF-1 enhances BMSC viability, migration, and anti-apoptosis in myocardial infarction via secreted frizzled-related protein 2 pathway. Stem Cell Res Ther. 2020;11(1):1–16.
50. Zhou W, Menkhorst E, Dimitriadis E. Jagged1 regulates endometrial receptivity in both humans and mice. FASEB J. 2021;35(8):e21784.
51. Masuda H, Anwar SS, Buhring HJ, Rao JR, Gargett CE. A novel marker of human endometrial mesenchymal stem-like cells. Cell Transplant. 2012;21(10):2201–14.
52. Pevsner-Fischer M, Levin S, Zipori D. The origins of mesenchymal stromal cell heterogeneity. Stem Cell Rev Rep. 2011;7(3):560–8.
53. Gao X, Murphy MM, Peyer JG, Ni Y, Yang M, Zhang Y, et al. Leptin receptor+ cells promote bone marrow innervation and regeneration by synthesizing nerve growth factor. Nat Cell Biol. 2023;25(12):1746–57.
54. Kara N, Xue Y, Zhao Z, Murphy MM, Comazzetto S, Lesser A, et al. Endothelial and Leptin Receptor(+) cells promote the maintenance of stem cells and hematopoiesis in early postnatal murine bone marrow. Dev Cell. 2023;58(5):348-60.e6.
55. Trinh T, Ropa J, Aljoufi A, Cooper S, Sinn A, Srour EF, et al. Leptin receptor, a surface marker for a subset of highly engrafting long-term functional hematopoietic stem cells. Leukemia. 2021;35(7):2064–75.
56. Deng M, Guerrero-Juarez CF, Sheng X, Xu J, Wu X, Yao K, et al. Lepr+ mesenchymal cells sense diet to modulate intestinal stem/progenitor cells via Leptin–Igf1 axis. Cell Research. 2022: 1–17.
57. Kobayashi H, Gieniec KA, Lannagan TR, Wang T, Asai N, Mizutani Y, et al. The origin and contribution of cancer-associated fibroblasts in colorectal carcinogenesis. Gastroenterology. 2022;162(3):890–906.
58. Lima-Couy I, Cervero A, Bonilla-Musoles F, Pellicer A, Simon C. Endometrial leptin and leptin receptor expression in women with severe/moderate endometriosis. MHR: Basic science of reproductive medicine. 2004;10(11):777–82.
59. Choi YS, Oh HK, Choi J-H. Expression of adiponectin, leptin, and their receptors in ovarian endometrioma. Fertility Sterility. 2013;100(1):135–41.
60. Gonçalves HF, Zendron C, Cavalcante FS, Aiceles V, Oliveira MAP, Manaia JHM, et al. Leptin, its receptor and aromatase expression in deep infiltrating endometriosis. J Ovar Res. 2015;8(1):1–7.
61. Yuan S-SF, Tsai K-B, Chung Y-F, Chan T-F, Yeh Y-T, Tsai L-Y, et al. Aberrant expression and possible involvement of the leptin receptor in endometrial cancer. Gynecol Oncol. 2004;92(3):769–75.
62. Boroń D, Nowakowski R, Grabarek BO, Zmarzły N, Opławski M. Expression pattern of leptin and its receptors in endometrioid endometrial cancer. J Clin Med. 2021;10(13):2787.
63. Kitawaki J, Koshiba H, Ishihara H, Kusuki I, Tsukamoto K, Honjo H. Expression of leptin receptor in human endometrium and fluctuation during the menstrual cycle. J Clin Endocrinol Metab. 2000;85(5):1946–50.
64. Méndez-López LF, Zavala-Pompa A, Cortés-Gutiérrez EI, Cerda-Flores RM, Davila-Rodriguez MI. Leptin receptor expression during the progression of endometrial carcinoma is correlated with estrogen and progesterone receptors. Arch Med Sci. 2017;13(1):228.
65. Dos Santos E, Serazin V, Morvan C, Torre A, Wainer R, de Mazancourt P, et al. Adiponectin and leptin systems in human endometrium during window of implantation. Fertil Steril. 2012;97(3):771–8.
66. Picó C, Palou M, Pomar CA, Rodríguez AM, Palou A. Leptin as a key regulator of the adipose organ. Rev Endocr Metab Disord. 2021. https://doi.org/10.1007/s11154-021-09687-5.
67. Clevers H, Watt FM. Defining adult stem cells by function, not by phenotype. Annu Rev Biochem. 2018;87:1015–27.
68. Ding L, Morrison SJ. Haematopoietic stem cells and early lymphoid progenitors occupy distinct bone marrow niches. Nature. 2013;495(7440):231–5.
69. Crane GM, Jeffery E, Morrison SJ. Adult haematopoietic stem cell niches. Nat Rev Immunol. 2017;17(9):573–90.
70. Pinho S, Frenette PS. Haematopoietic stem cell activity and interactions with the niche. Nat Rev Mol Cell Biol. 2019;20(5):303–20.
71. Bjornson CR, Cheung TH, Liu L, Tripathi PV, Steeper KM, Rando TA. Notch signaling is necessary to maintain quiescence in adult muscle stem cells. Stem Cells. 2012;30(2):232–42.
72. Mourikis P, Sambasivan R, Castel D, Rocheteau P, Bizzarro V, Tajbakhsh S. A critical requirement for notch signaling in maintenance of the quiescent skeletal muscle stem cell state. Stem Cells. 2012;30(2):243–52.
73. Calvi L, Adams G, Weibrecht K, Weber J, Olson D, Knight M, et al. Osteoblastic cells regulate the haematopoietic stem cell niche. Nature. 2003;425(6960):841–6.
74. Butler JM, Nolan DJ, Vertes EL, Varnum-Finney B, Kobayashi H, Hooper AT, et al. Endothelial cells are essential for the self-renewal and repopulation of Notch-dependent hematopoietic stem cells. Cell Stem Cell. 2010;6(3):251–64.
75. Zhu TS, Costello MA, Talsma CE, Flack CG, Crowley JG, Hamm LL, et al. Endothelial cells create a stem cell niche in glioblastoma by providing NOTCH ligands that nurture self-renewal of cancer stem-like cells. Cancer Res. 2011;71(18):6061–72.
76. Wang W, Yu S, Zimmerman G, Wang Y, Myers J, Yu VW, et al. Notch receptor-ligand engagement maintains hematopoietic stem cell quiescence and niche retention. Stem Cells. 2015;33(7):2280–93.
77. Dallas MH, Varnum-Finney B, Delaney C, Kato K, Bernstein ID. Density of the Notch ligand Delta1 determines generation of B and T cell precursors from hematopoietic stem cells. J Exp Med. 2005;201(9):1361–6.
78. Zhang S, Chan RW, Ng EH, Yeung WS. The role of Notch signaling in endometrial mesenchymal stromal/stem-like cells maintenance. Commun Biol. 2022. https://doi.org/10.1038/s42003-022-04044-x.
79. Bowers M, Zhang B, Ho Y, Agarwal P, Chen C-C, Bhatia R. Osteoblast ablation reduces normal long-term hematopoietic stem cell self-renewal but accelerates leukemia development. Blood. 2015;125(17):2678–88.
80. Relaix F, Rocancourt D, Mansouri A, Buckingham M. A Pax3/Pax7-dependent population of skeletal muscle progenitor cells. Nature. 2005;435(7044):948–53.
81. Lepper C, Partridge TA, Fan C-M. An absolute requirement for Pax7-positive satellite cells in acute injury-induced skeletal muscle regeneration. Development. 2011;138(17):3639–46.
82. Bouche A, Borner B, Richard C, Grand Y, Hannouche D, Laumonier T. In vitro-generated human muscle reserve cells are heterogeneous for Pax7 with distinct molecular states and metabolic profiles. Stem Cell Res Ther. 2023;14(1):243.
83. Kawaguchi D, Furutachi S, Kawai H, Hozumi K, Gotoh Y. Dll1 maintains quiescence of adult neural stem cells and segregates asymmetrically during mitosis. Nat Commun. 2013;4(1):1880.
84. Zhang H, Shang R, Bi P. Feedback regulation of Notch signaling and myogenesis connected by MyoD–Dll1 axis. PLoS Genet. 2021;17(8):e1009729.

Publisher's Note